The Plant Cell, Vol. 23: 3007–3025, August 2011, www.plantcell.org

Vacuolar Transport in Tobacco Leaf Epidermis Cells Involves a Single Route for Soluble Cargo and Multiple Routes for Membrane Cargo [W]

Francesca Bottanelli, Ombretta Foresti, Sally Hanton,[1] and Jürgen Denecke[2]

Centre for Plant Sciences, Faculty of Biological Sciences, University of Leeds, Leeds LS2 9JT, United Kingdom

We tested if different classes of vacuolar cargo reach the vacuole via distinct mechanisms by interference at multiple steps along the transport route. We show that nucleotide-free mutants of low molecular weight GTPases, including Rab11, the Rab5 members Rha1 and Ara6, and the tonoplast-resident Rab7, caused induced secretion of both lytic and storage vacuolar cargo. In situ analysis in leaf epidermis cells indicates a sequential action of Rab11, Rab5, and Rab7 GTPases. Compared with Rab5 members, mutant Rab11 mediates an early transport defect interfering with the arrival of cargo at prevacuoles, while mutant Rab7 inhibits the final delivery to the vacuole and increases cargo levels in prevacuoles. In contrast with soluble cargo, membrane cargo may follow different routes. Tonoplast targeting of an α-TIP chimera was impaired by nucleotide-free Rha1, Ara6, and Rab7 similar to soluble cargo. By contrast, the tail-anchored tonoplast SNARE Vam3 shares only the Rab7-mediated vacuolar deposition step. The most marked difference was observed for the calcineurin binding protein CBL6, which was insensitive to all Rab mutants tested. Unlike soluble cargo, α-TIP and Vam3, CBL6 transport to the vacuole was COPII independent. The results indicate that soluble vacuolar proteins follow a single route to vacuoles, while membrane spanning proteins may use at least three different transport mechanisms.

INTRODUCTION

Although the vacuolar branch of the plant secretory pathway has been studied intensively, it remains the most controversial and debated subject in the field. Dense vesicle (DV) carriers for the transport of storage proteins were first identified by Chrispeels in 1983 (Chrispeels, 1983). More than a decade later, Paris and colleagues introduced the concept that lytic and storage types of vacuoles could coexist within the same cell (Paris et al., 1996). This was supported by the notion that two types of vesicle (DV and clathrin-coated vesicles) mediated transport of storage proteins and acid hydrolases (Hohl et al., 1996).

Evidence suggesting multiple vacuolar sorting pathways was drawn from the large variety of vacuolar sorting signals (VSSs) operating in plants, differential sensitivities to the drugs Wortmannin and Brefeldin A (BFA), and differential ligand binding specificities of plant vacuolar sorting receptors (VSRs) (Gomez and Chrispeels, 1993; Kirsch et al., 1994; Matsuoka et al., 1995; Kirsch et al., 1996; Ahmed et al., 2000; Cao et al., 2000; Frigerio et al., 2008). More recently, this idea was further supported by VTi11, VTi12, and VPS45 gene knockouts, which appeared to affect vacuolar cargo in a differential manner (Sanmartín et al., 2007; Zouhar et al., 2009). However, this abundance of evidence is matched by a similar number of observations arguing against multiple vacuolar sorting pathways. The drug Wortmannin (Pimpl et al., 2003) and *Arabidopsis thaliana* VSRs knockouts (Shimada et al., 2003; Craddock et al., 2008) were later shown to affect the different types of VSS cargo indiscriminately. Although different types of vacuoles may coexist within certain plant cell types, a unifying model has not been drawn yet on how many different routes mediate transport to the vacuoles (Frigerio et al., 2008).

One of the problems with the early work is that conclusions were drawn from the use of a single effector or gene knockdown. If two vacuolar cargo molecules exhibit different binding affinity to the same receptor, simple differences in the dose response can be misinterpreted as true differential effects. Another problem arises from the large number of transport steps required to complete passage from the endoplasmic reticulum (ER) to the vacuole. Branching points may occur at different positions in the pathway, but two divergent routes may merge again before the vacuole. To increase the chances of detecting a branching point, it is therefore important to dissect the individual steps systematically along the pathway.

For over a decade, low molecular weight Rab GTPases have become a major tool for disrupting specific steps in the secretory pathway (Rutherford and Moore, 2002). Nucleotide-deficient mutants of plant Rab5 have been efficiently used to interfere with vacuolar transport and have been localized to the prevacuolar compartment (PVC) (Sohn et al., 2003; Bolte et al., 2004; Kotzer et al., 2004). Ara6 is an unusual member of the Rab5 GTPase family that differs from the canonical forms Rha1 and Ara7 by being membrane anchored via N-terminal myristoylation instead of C-terminal prenylation (Ueda et al., 2001). To expand the number of tools available to dissect vacuolar sorting, Rab

[1] Current address: Aintree University Hospitals NHS Trust, Longmoor Lane, Liverpool L9 7AL, UK.
[2] Address correspondence to j.denecke@leeds.ac.uk.
The author responsible for distribution of materials integral to the findings presented in this article in accordance with the policy described in the Instructions for Authors (www.plantcell.org) is: Jürgen Denecke (j.denecke@leeds.ac.uk).
[W] Online version contains Web-only data.
www.plantcell.org/cgi/doi/10.1105/tpc.111.085480

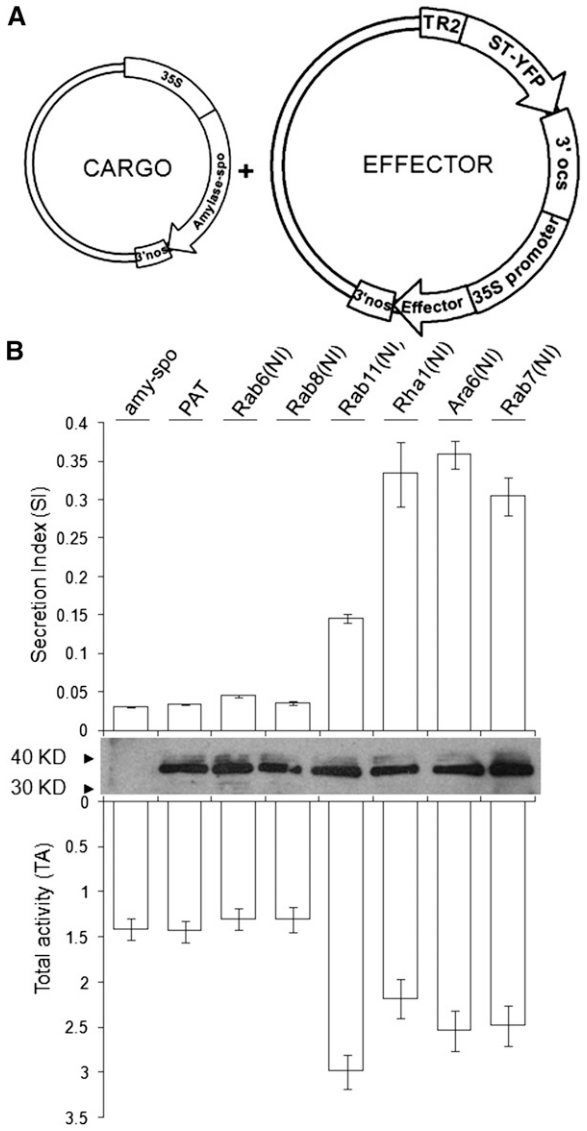

Figure 1. Nucleotide-Free Rab11, Rha1, Ara6, and Rab7 Interfere with the Trafficking of the Vacuolar Cargo Amy-Spo.

(A) A dual expression vector (Effector) was used in conjunction with a plasmid harboring the vacuolar cargo amy-spo (Cargo) to test for interference with vacuolar sorting. In the dual expression vector, the Golgi marker ST-YFP was used as internal reference for normalization of the transfection efficiency, and untagged Rab GTPase mutants (Effector) are present in the same cassette.

(B) Tobacco protoplasts were cotransfected with a constant amount of plasmid harboring the vacuolar cargo amy-spo alone (15 μg, first lane) or together with constant amounts (30 μg) of plasmids harboring either the mock effector PAT or a nucleotide-deficient mutant [Rab(NI)] as indicated above each lane. After a 24-h incubation, cells and medium were harvested, and the α-amylase activity was measured in each fraction. The SI (top panel) was calculated as the ratio between extracellular and intracellular activities. Rab11(NI), Rha1(NI), Ara6(NI), and Rab7(NI) caused secretion of the vacuolar cargo into the medium. The level of expression of the various untagged effectors was equalized via immunoblots aimed at detecting ST-YFP present in the same expression cassette. Total activities (TA) are shown (bottom panel) to illustrate that induced secretion was not due to cell mortality (notice that total levels are increased when vacuolar sorting was impaired due to higher stability of amy-spo in the medium compared with the vacuole). Error bars represent standard errors from five independent transfections for each condition.

GTPases were chosen that would operate at the organelles flanking the PVC in the pathway. Plant Rab6 (Osterrieder et al., 2009) and Rab8 (Zheng et al., 2005; Speth et al., 2009) were shown to localize to the Golgi apparatus, while Rab11 members have been localized to the trans-Golgi network (TGN) and the cell plate (Ueda et al., 1996; Preuss et al., 2006; Chow et al., 2008). Last along the pathway is Rab7, which has been used as a marker for the vacuolar membrane in various instances (Saito et al., 2002; Uemura et al., 2002). A potential role of Rab7 in vacuolar sorting has not been investigated to date.

In this work, a systematic screening of mutants based on interference with the trafficking of a vacuolar biochemical cargo identified Rab11, Rha1, Ara6, and Rab7 mutants as effectors that dissect distinct events in vacuolar sorting. Comparison of different classes of vacuolar cargo suggests that tobacco (*Nicotiana tabacum*) epidermis cells use a single route for soluble proteins. By contrast, membrane proteins can use divergent routes and may segregate from other vacuolar cargo at multiple steps along the pathway.

RESULTS

Identification of Rab GTPases Involved in Vacuolar Sorting

Nucleotide binding mutants of Rab GTPases have been instrumental in blocking ER export (Batoko et al., 2000) and vacuolar sorting (Bolte et al., 2004). In this study, the Asn-to-Ile substitution (NI) in the nucleotide binding domain was chosen for a systematic comparison as it was shown to lead to a dominant-negative phenotype by titration of the exchange factors involved (Jones et al., 1995; Richardson et al., 1998). NI mutants of the Golgi Rab6 and Rab8, TGN Rab11, PVC Rha1 and Ara6, and the tonoplast Rab7 were thus created in an attempt to interfere with sorting steps at different levels along the pathway.

To permit routine quantification and dose–response analysis of different GTPase mutants, a dual expression (DV) vector was developed (Figure 1A) for the simultaneous expression of untagged effectors and the Golgi marker the N terminus of sialyl-transferase fused to yellow fluorescent protein (ST-YFP) under control of the TR2′ promoter (Velten et al., 1984). By first quantifying the Golgi marker ST-YFP via immunoblotting, it was possible to equalize the transfection efficiency for individual plasmids and enabled control over the level of expression of the various untagged Rab mutants.

Initial screening of Golgi-, TGN-, PVC-, and tonoplast-localized Rabs was aimed at monitoring induced secretion of the vacuolar cargo α-amylase-sporamin (amy-spo), a fusion protein carrying the VSS of sweet potato (*Ipomoea batatas*) sporamin, which has been extensively tested (Pimpl et al., 2003; daSilva et al., 2005). Constant amounts of amy-spo encoding plasmid were coelectroporated in tobacco protoplasts together with the double

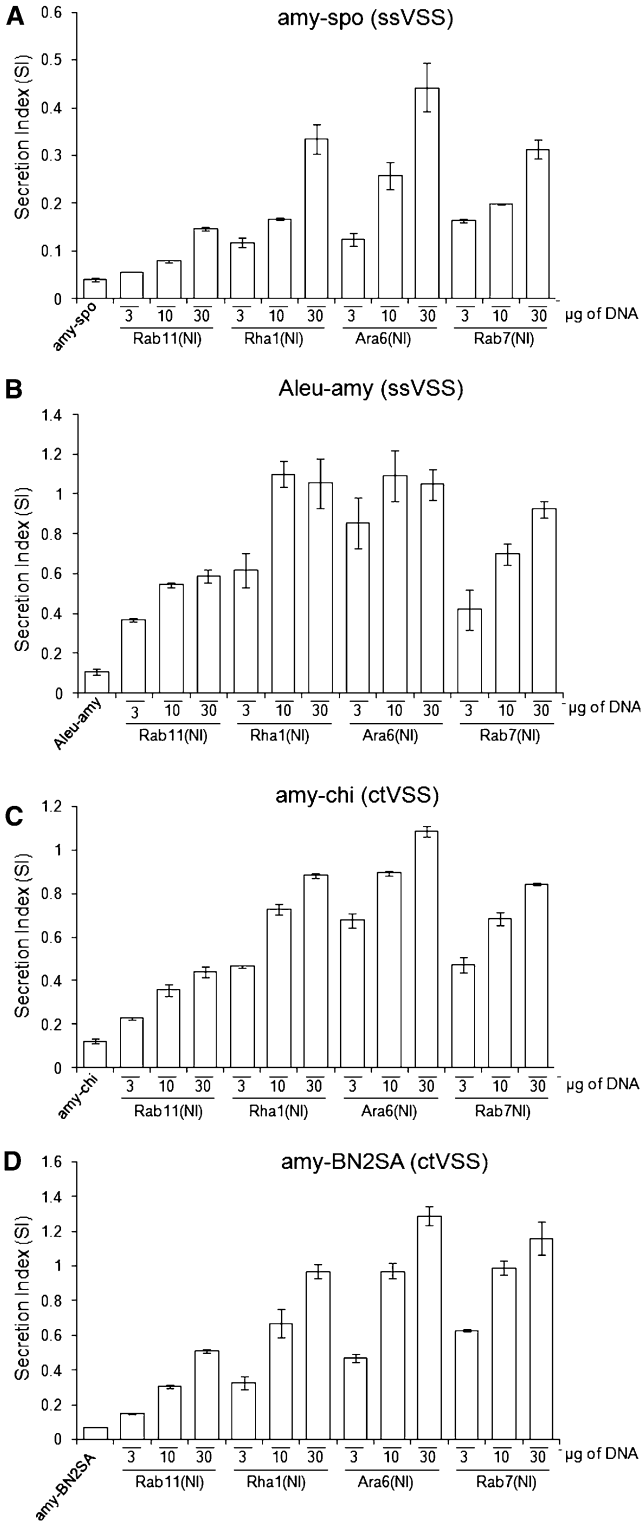

Figure 2. Interference with Post-Golgi Rab GTPase Activity Highlights a Single Route to the Vacuole for ssVSS and ctVSS Cargo.

Tobacco protoplasts were cotransfected with a constant amount of plasmid (15 μg) encoding either ssVSS cargo amy-spo **(A)** and Aleu-amy **(B)** or the ctVSS cargo amy-chi **(C)** and amy-BN2SA **(D)** alone (first lane) or together with increasing concentrations of either Rab11(NI), Rha1(NI), Ara6(NI), and Rab7(NI) harboring plasmids as indicated below each lane. α-Amylase assays and routine verification of ST-YFP by immunoblotting was performed as described in Figure 1. Error bars represent standard errors from five independent transfections for each condition.

expression vectors harboring the various nucleotide-deficient NI mutants [Rab(NI)]. As a mock effector, the gene encoding the cytosolic phosphinothricin acetyltransferase (PAT) replaced the various GTPase coding regions in the dual expression construct to serve as wild-type background. Cells and medium were harvested and the α-amylase activity was measured in each fraction, followed by the calculation of the ratio between the extracellular and intracellular activities, referred to as the secretion index (SI).

As shown in Figure 1B, expression levels of the internal marker ST-YFP were comparable in each case, and the differential effects of the various mutant GTPases could therefore be attributed to the specific role of the GTPases in the pathway. NI mutants of the Golgi Rab GTPases Rab6 and Rab8 had no influence on the trafficking of the cargo amy-spo, suggesting that they may not be involved in vacuolar sorting steps. Surprisingly, Rab11(NI) expression led to a modest but reproducible increase in the secretion of the vacuolar cargo, indicating a possible role in the transport of vacuolar proteins. Rha1(NI), Ara6(NI), and Rab7 (NI) caused a strong inhibitory effect on the vacuolar trafficking of amy-spo as indicated by a ~10× increase in the SI. Figure 1B shows that none of the total α-amylase activities (medium + cells) is reduced, thus ruling out cell mortality as a cause for induced secretion. By contrast, an increase in the total activity was seen in samples where vacuolar sorting was inhibited, which is explained by a higher stability of the reporter in the culture medium compared with the vacuole (Foresti et al., 2006).

Soluble Proteins Reach the Vacuole via a Single Route

The positive candidates Rab11(NI), Rha1(NI), Ara6(NI), and Rab7 (NI) were chosen from the initial screening to perform a more detailed dose–response analysis and to compare vacuolar cargo harboring different classes of VSS, including the so-called sequence-specific VSS (ssVSS) and C-terminal VSS (ctVSS). These two classes have been proposed to follow different pathways to either lytic or storage vacuoles, respectively (Matsuoka et al., 1995; Sanmartín et al., 2007; Zouhar et al., 2009).

Initially a dose–response analysis was performed with the ssVSS cargo amy-spo in an attempt to monitor any subtle dose-dependent difference that was not highlighted in the initial screening. Tobacco protoplasts were thus cotransfected with constant amounts of amy-spo encoding plasmid together with increasing quantities of plasmids encoding either Rab11(NI), Rha1(NI), Ara6 (NI), or Rab7(NI) (Figure 2A). All four dominant-negative (NI) mutants caused a dose-dependent increase in the SI. The TGN Rab11(NI) had the weakest effect on amy-spo trafficking as shown by an approximately sixfold increase in the SI for the highest concentration of effector. Increasing doses of Rha1(NI), Ara6(NI), and Rab7(NI) caused stronger, dose-dependent inductions of secretion that reached ~10-fold the basal secretion level of the

cargo model in the case of both Rha1(NI) and Rab7(NI) and ~13-fold in the case of the nucleotide-free Ara6.

To expand the portfolio of ssVSS cargo, we generated a fusion bearing the barley (*Hordeum vulgare*) aleurain propeptide sequence (Di Sansebastiano et al., 2001) at the N terminus of α-amylase (Aleu-amy). The new cargo was tested against the same inhibitors as in Figure 1A. The basal level of secretion of Aleu-amy alone was approximately threefold higher compared with amy-spo, indicating a lower transport fidelity. Figure 2B shows that secretion of Aleu-amy was induced by the same post-Golgi Rab mutants as amy-spo, and again Rab11(NI) was the weakest effector (cf. Figures 2A and 2B). The only difference was a faster induction at low effector concentrations in all four cases and a higher maximum induced secretion. This could simply be explained by a lower affinity of the aleurain signal for the same receptor. No differential sensitivity was observed.

In an attempt to highlight any difference in the trafficking of ssVSS and ctVSS cargo, a fusion between α-amylase and the C-terminal processed fragment from tobacco chitinase A (amy-chi) was created. The resulting chimera contains the heptapeptide GLLVDTM exposed at the C terminus, which was shown to be sufficient for chitinase transport to the storage vacuole (Neuhaus et al., 1991). In comparison to amy-spo, amy-chi shows a higher basal level of secretion, similar to that of Aleu-amy. Figure 2C shows that the dose response to coexpressed Rab11(NI), Rha1(NI), Ara6(NI), and Rab7(NI) revealed an almost identical pattern as the two previous cargo molecules, except for a closer resemblance to the pattern observed for Aleu-amy (Figure 2B).

One further α-amylase fusion was generated containing the ctVSS from 2S storage albumin from Brazil nut (*Bertholletia excelsa*) (amy-BN2SA). The resulting chimera contains the 14 C-terminally located residues SPMRCPMGGSIAGF, which were earlier shown to be sufficient for its sorting to the vacuole (Saalbach et al., 1996). Amy-BN2SA showed an intermediate transport fidelity under control conditions and showed approximately twofold higher basal levels of secretion compared with amy-spo (Figure 2D). In addition, the resulting dose–response pattern was again comparable to those observed for the other cargo molecules amy-spo, Aleu-amy, and amy-chi.

To obtain evidence for two distinct pathways, it would be necessary to identify two inhibitors, of which one interfered with vacuolar sorting of ssVSS-cargo but not ctVSS cargo while the other displayed the reciprocal specificity. None of the post-Golgi Rab dominant-negative mutants could highlight such polarized differences in the trafficking of ssVSS and ctVSS cargo. This suggests that there may be only one route for soluble proteins leading to the vacuole in tobacco leaf protoplasts.

In Situ Analysis of Soluble Vacuolar Cargo in Leaf Epidermis Cells

Although NI mutants of Rab11, Rab5, and Rab7 all caused secretion of soluble vacuolar cargo, the position in the pathway at which they interfere is likely to be different. The in vivo biochemical assays based on the use of α-amylase fusions is a valuable tool to monitor transport of soluble cargo quantitatively. However, it distinguishes only between intracellular and extracellular partitioning of cargo. To detect intracellular transport intermediates en route to the vacuole, fluorescently tagged vacuolar cargo can be visualized in situ using confocal laser scanning microscopy. Soluble red fluorescent protein (RFP) has recently been shown to be an excellent reporter for microscopy under acidic conditions found in the vacuoles (Hunter et al., 2007). The soluble cargo molecules Aleu-amy and amy-chi used in the biochemical approach were thus replaced by their respective RFP chimeras Aleu-RFP (Foresti et al., 2010) and RFP-chi.

To carry out in situ analysis on single cells expressing visible cargo molecules and invisible (untagged) Rab mutants, we wanted to use the dual expression cassettes harboring the various untagged effectors and the internal Golgi marker ST-YFP (Figure 1A). To demonstrate that cotransformation from a single T-DNA is effective, we created a dual color expression vector (pRainbow) encoding YFP-labeled plasma membrane marker and an RFP-labeled tonoplast marker on a single T-DNA. Tobacco leaf infiltration with the new *Agrobacterium tumefaciens* strain followed by extensive image analysis revealed that cells exhibited the typical variance in expression levels due to differences in the actual time of transformation after infiltration or resulting from insertion copy number variability and position effects. However, we have not found a single cell in which one of the two colors was missing, suggesting that the cotransformation from a single T-DNA was highly efficient. Moreover, fluorescence intensity from the two markers was highly correlated, verified by a constant red-green ratio that was independent of expression level (see Supplemental Figure 1 online).

Dual expression cassettes (Figure 1A) were subcloned into binary vectors for *Agrobacterium*-mediated plant transformation. After *Agrobacterium* leaf infiltration, the dual expression vectors permitted efficient identification of cells guaranteed to express Rab(NI) by simple visualization of the Golgi marker encoded by the same T-DNA. Tobacco leaves were thus coinfiltrated with an *Agrobacterium* strain encoding for Aleu-RFP together with the various dual expression vectors for ST-YFP and the effectors (DVST-YFP+effector). A control vector containing the mock effector PAT instead of Rab(NI) was also included to represent wild-type background. Only cells that showed mobile yellow fluorescent Golgi bodies labeled with ST-YFP (shown in green) were imaged, and altered distribution of Aleu-RFP (shown in purple) was documented (Figure 3).

To evaluate vacuole-to-apoplast repartitioning, infiltrated leaf epidermis tissue was imaged at low magnification with the focal plane in the center of the cells. Figure 3A shows that Aleu-RFP labels the central vacuole when expressed with the mock effector PAT. This confirms that neither the Golgi marker ST-YFP nor cytosolic PAT perturbs vacuolar trafficking. It also shows that the fidelity of Aleu-RFP sorting is very high, as the apoplast remains nonfluorescent (white arrowheads). By contrast, when Aleu-RFP is coexpressed together with the nucleotide-deficient mutant of Rab11, it is readily detected in the apoplast (Figure 3B, white arrowheads) at the expense of a portion of vacuolar fluorescence, which was reduced. Coexpression with the NI mutants of Rha1 (Figure 3C), Ara6 (Figure 3D), or Rab7 (Figure 3E) caused more severe mis-sorting of Aleu-RFP to the apoplast of the cells. Although microscopy provides more qualitative results, they do confirm the earlier biochemical experiments (Figures 1 and 2).

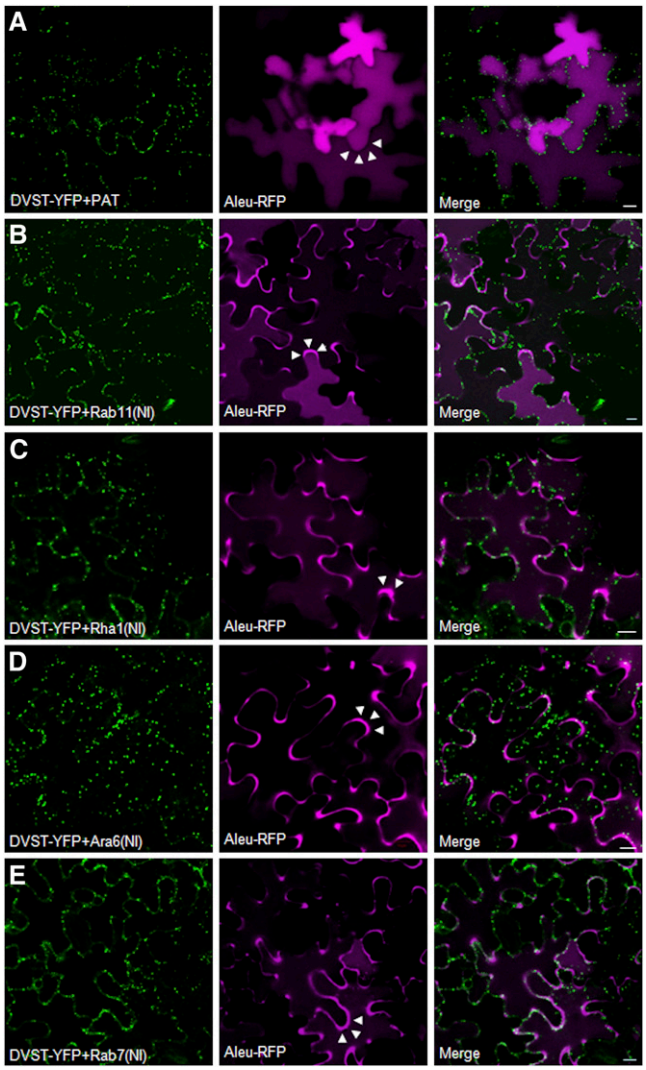

Figure 3. The Fluorescent Chimera Aleu-RFP Is Redirected to the Apoplast in the Presence of Nucleotide-Free Variants of Rab11, Rha1, Ara6, and Rab7.

An *Agrobacterium* strain harboring an Aleu-RFP encoding plasmid was infiltrated together with the strain harboring the dual expression vectors encoding for the Golgi marker ST-YFP together with either PAT **(A)** as mock effector or Rab11(NI) **(B),** Rha1(NI) **(C)**, Ara6(NI) **(D)**, or Rab7(NI) **(E)** mutants as test objects.

(A) Cells expressing comparable levels of the internal standard ST-YFP were chosen for imaging the midsection of the lower epidermis to evaluate both vacuolar and apoplastic fluorescence of Aleu-RFP where appropriate. The mock effector PAT does not prevent normal vacuolar localization of Aleu-RFP, as shown by diffuse fluorescence in the central vacuole and an absence of signal in the apoplast (white arrow heads).

(B) to **(E)** Rab11(NI), Rha1(NI), Ara6(NI), and Rab7(NI) mutants cause mis-sorting of Aleu-RFP to the apoplast of the cells (white arrowheads). Bars = 10μm.

To detect Aleu-RFP in transit to the vacuole, tissues analyzed in Figure 3 were imaged at high magnification with the focal plane at the cell cortex to image the thin layer of cytosol in between the apical membrane and the tonoplast. Figure 4A shows that in addition to the Golgi marker ST-YFP, extra-Golgi structures were labeled by Aleu-RFP when coexpressed with the mock effector. Coexpression of the NI mutant of Rab11 caused a noticeable reduction in punctate Aleu-RFP labeling (Figure 4B). By contrast, coexpression with Rha1(NI), Ara6(NI), and in particular Rab7(NI) led to more numerous and brighter fluorescent extra-Golgi structures (Figures 4C to 4E).

To express quantitatively the decrease or increase in Aleu-RFP fluorescence in post-Golgi structures, fluorescent signals were quantified by manual masking of all punctate structures using ImageJ (Abramoff et al., 2004) from various images comprising at least 20 different cells and/or 400 individual punctae followed by Pearson-Spearman correlation (PSC) analysis (French et al., 2008). The resulting scatterplots comprise all the data for each series and are shown on the right-hand side of a representative image. PSC correlation coefficients were close to 0 or even negative, as expected when comparing Golgi and post-Golgi organelles. However, the Golgi fluorescence serves as reference point to monitor changes in the abundance of cargo in post-Golgi organelles. Subsequent quantification of all pixels in the scatterplots permitted calculation of a ratio indicating the amount of punctate Aleu-RFP fluorescence (shown in red) against the Golgi marker ST-YFP as internal marker (shown in green). This ratio (top right corner) is reduced for the Rab11 (NI) coexpression experiment and shows a reduced number of red-only pixels near the *x* axis. By contrast, the two mutant Rab5 GTPases, and in particular the mutant Rab7, caused an increase in the red-green ratio. This is an important result as it indicates clear differences between the different classes of Rab mutants.

An RFP-chitinase chimera (RFP-chi) was also tested against the same portfolio of inhibitors to represent the ctVSS cargo class. The mock transfection with PAT shows that the fidelity of transport is lower compared with Aleu-RFP (Figure 3A). RFP-chi faintly labels the central vacuole and also labels the cell periphery (Figure 5A). This was not observed for Aleu-RFP (Figure 3A). When imaged at the cell cortex, the peripheral fluorescence was shown to represent RFP-chi in the ER (Figure 5B). In addition, small mobile punctate structures could also be observed (white arrowheads), but they were harder to detect compared with those highlighted by Aleu-RFP (Figure 4A). These results suggest that in addition to a lower transport fidelity leading to partial secretion (Figure 2C), the chitinase signal also appears to lead to partial ER retention. This was independent of the expression levels and/or timing of the experiment.

When coexpressed with NI mutants of the various Rab GTPases, the same trend was observed as for Aleu-RFP. Nucleotide-free Rab11 mediated a decrease in the red-green ratio and reduced the red fluorescence in the punctate structures (Figure 5C). By contrast, the two Rab5 mutants Rha1(NI) and Ara6(NI) caused a stronger accumulation of RFP-chi in post-Golgi structures as shown by an increase in the red/green ratio and a better defined red fluorescent cloud of punctae (Figures 5D and 5E). The strongest inhibitory effect and most

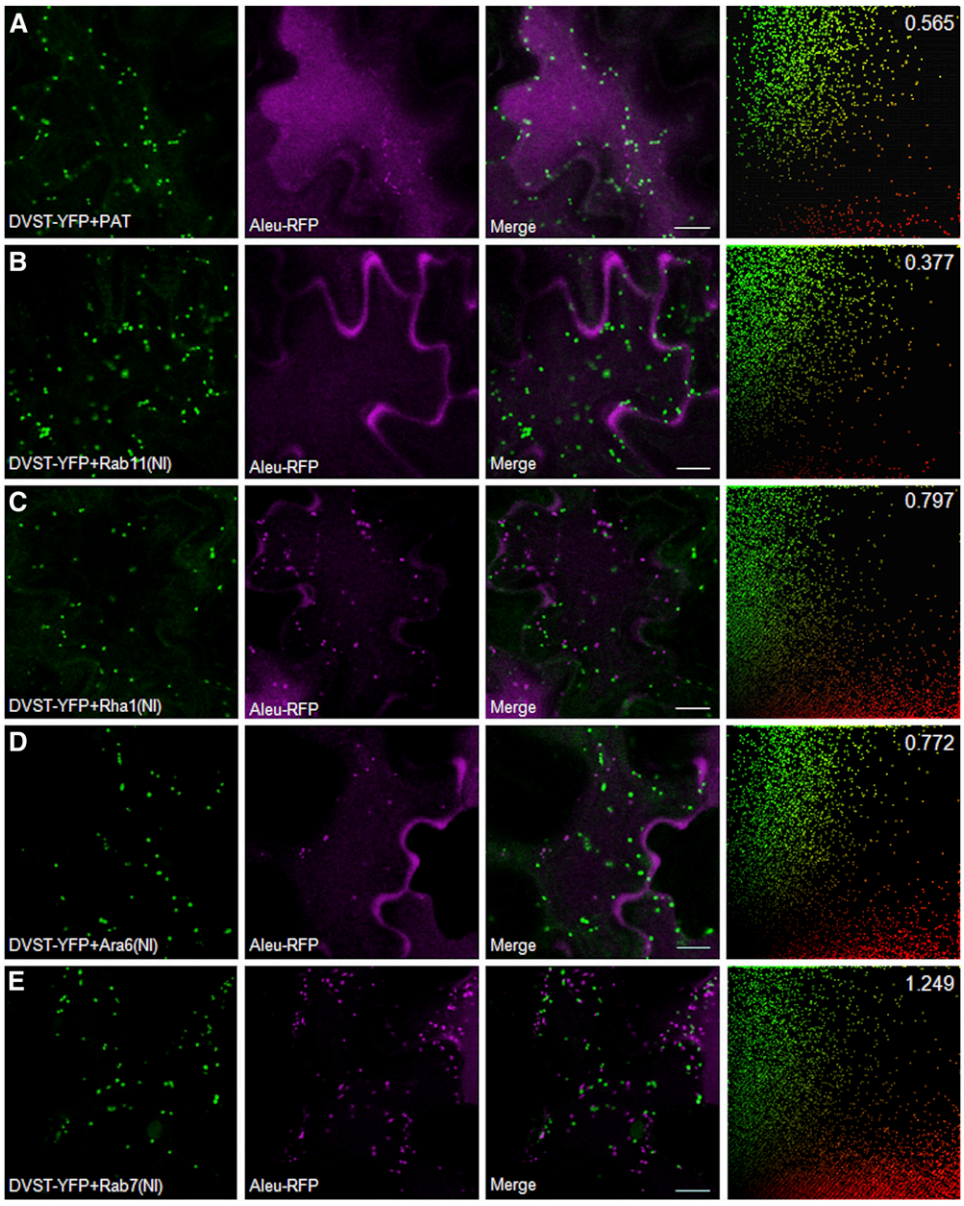

Figure 4. Rha1, Ara6, and Rab7 Mutants Cause Accumulation of Aleu-RFP in Post-Golgi Structures.

The same samples analyzed in Figure 3 were imaged at the cell cortex at higher magnification to visualize individual organelles in the cytosol and to assess accumulation of Aleu-RFP (purple) in intracellular compartments in transit to the vacuole. The far right panels show scatterplots derived from the correlation analysis performed using the PSC plug-in for ImageJ (French et al., 2008) and show ST-YFP signals in green and Aleu-RFP signals in red rather than purple due to software characteristics. At least 400 individual punctate structures were manually masked on a minimum of 20 independent images or 400 independent punctae for each coexpression pair. The overall sum of green and red pixels was quantified, and the red/green ratio was calculated and is shown in the top right corner. Notice that in all cases, the vacuolar marker Aleu-RFP can be visualized in post-Golgi punctate structures in transit to the vacuole, as no overlap with the Golgi-marker was detected, but the amount of post-Golgi red fluorescence relative to the internal marker ST-YFP is increased in **(C)** and **(D)** and particularly **(E)**. Bars = 10μm.

pronounced accumulation of red fluorescent post-Golgi organelles was again observed when Rab7(NI) was coexpressed (Figure 5F) .

The results confirm that ssVSS cargo and ctVSS cargo show the same sensitivity toward the various effectors. They also illustrate that the individual Rab GTPases may interfere at different steps of the pathway, even though all cause induced secretion of soluble vacuolar cargo. The reduced post-Golgi fluorescence caused by the Rab11 mutant may indicate an early transport defect, interfering with arrival of Aleu-RFP at the TGN and/or PVC. Both Rab5 (NI) and Rab7(NI) caused an increase in post-Golgi fluorescence, but the stronger effect of the latter suggests that a late transport

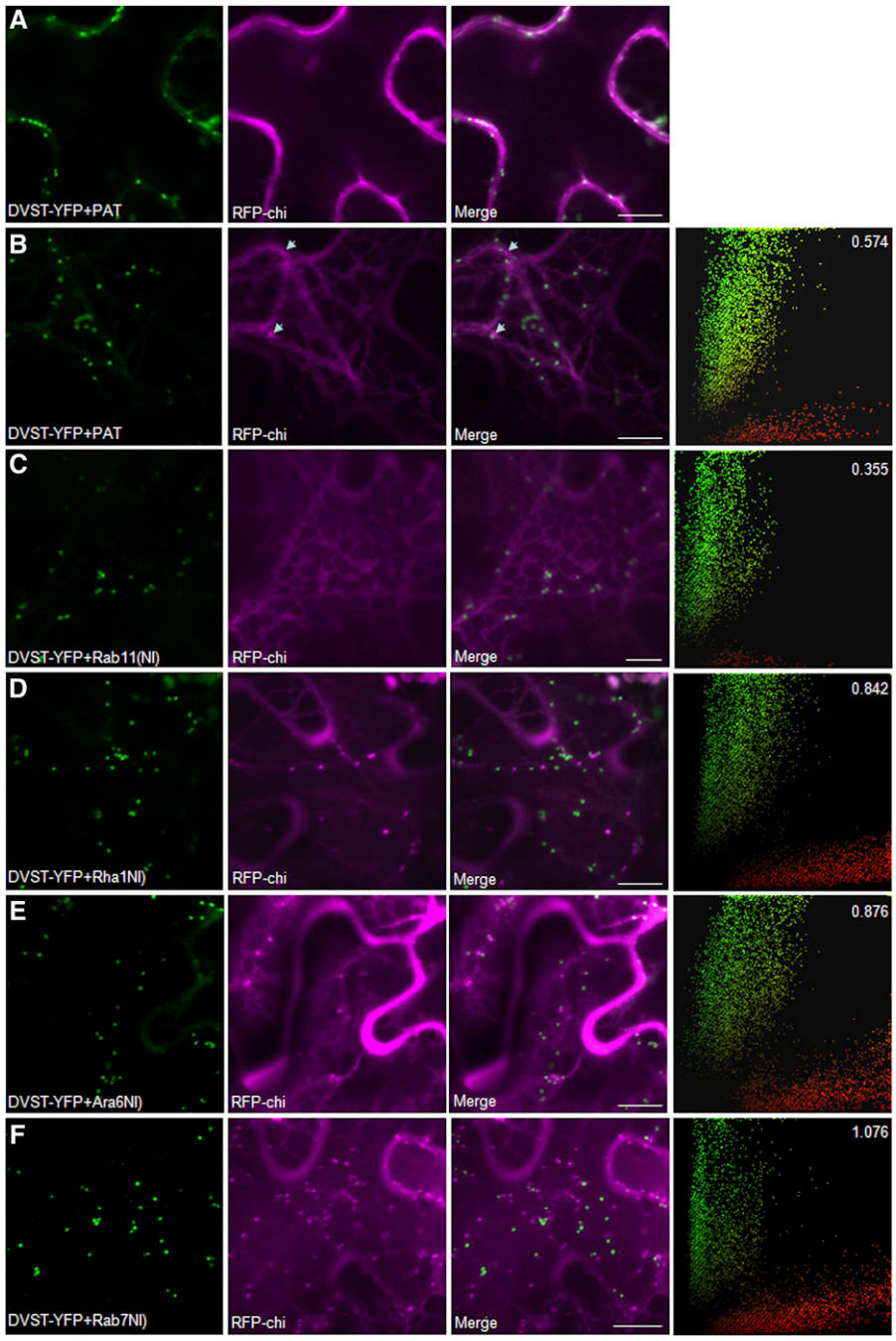

Figure 5. RFP-Chi Transport Shows the Same Sensitivity toward Rab Mutants as Aleu-RFP Does.

The trafficking of the ctVSS fluorescent chimera RFP-chi was tested against the same Rab mutants using experimental conditions as in Figure 4 and subjected to the same statistical testing. In the presence of the mock effector PAT, RFP-chi is partially detected in the central vacuole **(A)** and in transit through the ER **(B)** as well as small extra-Golgi punctae (**[B]**; indicated by arrows). Coexpression with Rab11(NI) shows RFP-chi mostly in the ER without punctate post-Golgi structures **(C)**. Rha1(NI), Ara6(NI), and particularly Rab7(NI) caused a strong accumulation of the chimera in post-Golgi structures (**[D]** to **[F]**). Bars = 10 μm.

step to the vacuole is compromised. However, it remains to be shown how this could lead to secretion of the vacuolar cargo.

Vacuolar Delivery of GFP-Vam3 Is Dependent on the Action of the Tonoplast GTPase Rab7

Distinct pathways for the transport of transmembrane and soluble proteins to the plant vacuole have been proposed based on work with the drug BFA, which is widely used as an ER export inhibitor. The drug prevented the soluble cargo phytohemagglutinin but not the membrane spanning cargo α-TIP from reaching the vacuole (Gomez and Chrispeels, 1993). Since membrane spanning proteins often display cytosolic portions, they can interact with different types of sorting machinery compared with soluble proteins which are confined to the lumen of the secretory pathway.

In an attempt to highlight any differences in the trafficking of soluble and membrane spanning cargo to the vacuole, the tonoplast SNARE Vam3(SYP22) was chosen for comparisons with the soluble markers. Vam3 is a tail-anchored transmembrane SNARE that has been extensively used as a tonoplast marker (Saito et al., 2002; Uemura et al., 2002) and a green fluorescent protein (GFP)-Vam3 fusion was previously shown not to interfere with vacuolar sorting (Foresti et al., 2006).

To analyze the effect of the various Rab mutants on the trafficking of membrane cargo, the experiments shown in Figures 3 to 5 were repeated using GFP-Vam3 as cargo instead of Aleu-RFP (Figure 6). Coexpression of GFP-Vam3 with the mock effector PAT (Figure 5A) or the (NI) mutant of Rab11 (Figure 6B) resulted in the typical tonoplast localization pattern observed previously for GFP-Vam3, displaying fluorescence at the delimiting vacuolar membrane and also in the so-called bulbs, bright fluorescent intravacuolar spherical structures with double or multiple folded vacuolar membranes (Saito et al., 2002; Uemura et al., 2002; Foresti et al., 2006). Coexpression with the two Rab5 members Rha1(NI) and Ara6(NI) did not affect labeling of the delimiting vacuolar membrane (Figures 6C and 6D). A clear phenotype is caused by coexpression with Rab7(NI), resulting in reduced fluorescence at the delimiting vacuolar membrane and formation of enlarged punctate structures (as indicated by arrowheads, Figure 6E). The latter accumulate GFP-Vam3 but remain totally distinct from a normal Golgi pattern highlighted by coexpressed ST-YFP. These enlarged structures were not observed upon coexpression with other Rab mutants (Figures 6A to 6D) regardless of the plane of focus.

The results indicate that GFP-Vam3 delivery to the delimiting vacuolar membrane is insensitive to NI mutants of Rab11 and Rab5 but strongly dependent on functional Rab7 GTPase. This suggests that Rab7 could mediate the very terminal step of vacuolar delivery of Vam3, consistent with Rab7 localization in the tonoplast (Saito et al., 2002).

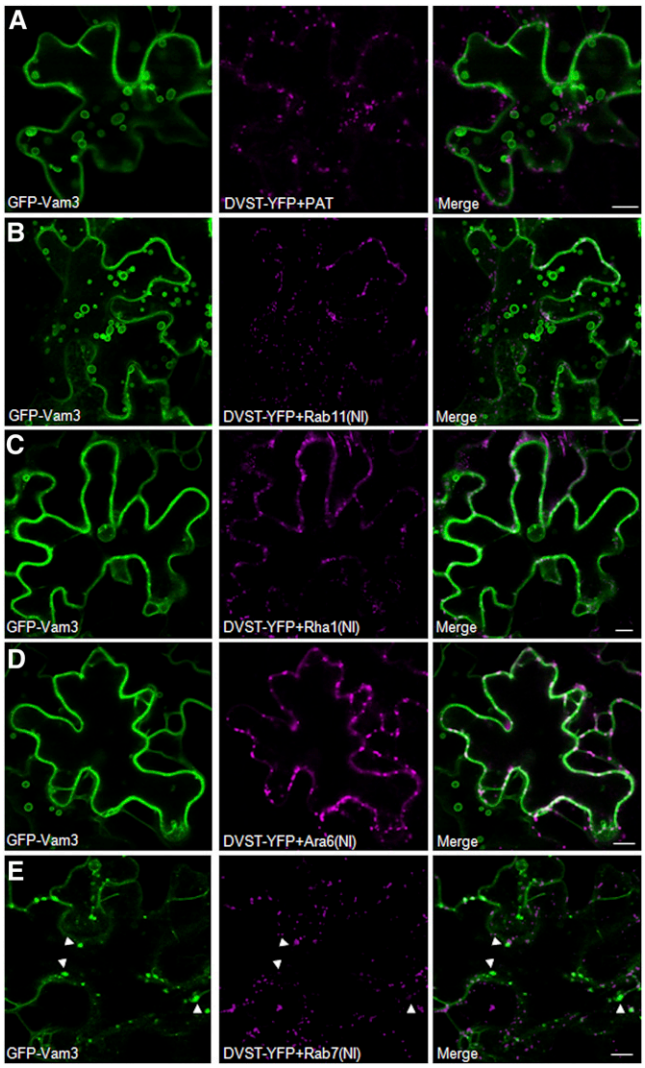

Figure 6. Dominant-Negative Rab7 Interferes with Vacuolar Delivery of GFP-Vam3.

Tobacco leaves were coinfiltrated with *Agrobacterium* strains harboring a GFP-Vam3–encoding plasmid together with the various dual expression vectors for ST-YFP and either PAT **(A)**, Rab11(NI) **(B)**, RHA1(NI) **(C)**, ARA6(NI) **(D)**, or Rab7(NI) **(E)** mutants. Bars = 10 μm.

(A) The mock transfection showed normal tonoplast labeling of GFP-Vam3 as observed before (Foresti et al., 2006).

(B) to **(D)** Expression of Rab11(NI) **(B)**, Rha1(NI) **(C)**, and Ara6(NI) **(D)** also failed to arrest trafficking of the chimera to the vacuolar membrane.

(E) Interestingly, GFP-Vam3 accumulated in enlarged punctate structures when Rab7(NI) was coexpressed (white arrowheads). GFP-Vam3 structures were always found separate from the Golgi marker ST-YFP, which showed an unaltered distribution.

While αTIP Trafficking Is Rab5 and Rab7 Sensitive, the Calcineurin B–Like Protein CBL6 Reaches the Vacuole in an Unconventional Manner

To compare the transport of GFP-Vam3 with other tonoplast markers, two further fluorescent chimeras were used. αTIP-YFP was used as a model protein for multiple membrane spanning domain proteins (Hunter et al., 2007). A member of the Calcineurin B–like protein family (CBL6) was chosen as an independent tonoplast marker as it was shown to localize to the vacuolar membrane in tobacco protoplasts and leaves (Luan et al., 2002; Batistic et al., 2010). Plant CBLs are divided into two groups, one of which is N-terminally myristoylated and plasma membrane

resident. CBL6 falls into the second class characterized by an N-terminal transmembrane domain (Batistic and Kudla, 2009). Moreover, CBL6 has been recently suggested to traffic to the vacuole via a COPII-independent pathway (Batistic et al., 2010), but its route has not been further characterized. A control experiment with tobacco leaf epidermis cells coexpressing the plasma membrane marker YFP-SYP121 (Foresti et al., 2006) and the newly constructed CBL6-RFP fusion confirms a typical tonoplast pattern from this chimeric gene that can be clearly distinguished from the plasma membrane (see Supplemental Figure 2 online).

To explore if αTIP-YFP and CBL6-RFP display the same sensitivity to the four Rab mutants used in this study, the dual expression vectors containing either the mock effector PAT or Rab11(NI), Rha1(NI), Ara6(NI), or Rab7(NI) mutants used in Figures 3 to 5 were reconstructed to replace the TR2′-driven internal Golgi marker ST-YFP with TR2′-driven CBL6-RFP. These constructs were then coexpressed with a separate strain encoding αTIP-YFP alone (Hunter et al., 2007). Cells displaying both red and yellow fluorescence were thus guaranteed to contain the various effector molecules and allow simultaneous comparison of the two membrane spanning proteins.

Figure 7A shows that coexpression with the mock effector PAT reveals a typical tonoplast pattern for both αTIP-YFP and CBL6-RFP. The same pattern was observed when Rab11(NI) was coexpressed (Figure 7B). By sharp contrast, coexpression with Rha1(NI), Ara6(NI), and Rab7(NI) caused significant retention of αTIP-YFP in punctate structures, while CBL6-RFP was unaffected (Figures 7C to 7E). No punctate CBL6-RFP structures could be detected regardless of the plane of focus.

The results indicate that αTIP-YFP traffics in a similar manner as soluble cargo because those effectors that mediated efficient retention of soluble cargo in punctate structures also mediated that same effect on the membrane cargo. By contrast, CBL6-RFP traffics to the tonoplast via a completely different route compared with either soluble cargo and αTIP-YFP or the tail-anchored GFP-Vam3. It can also be concluded that the vacuolar compartment is still intact under conditions where vacuolar sorting of a subset of vacuolar markers is inhibited.

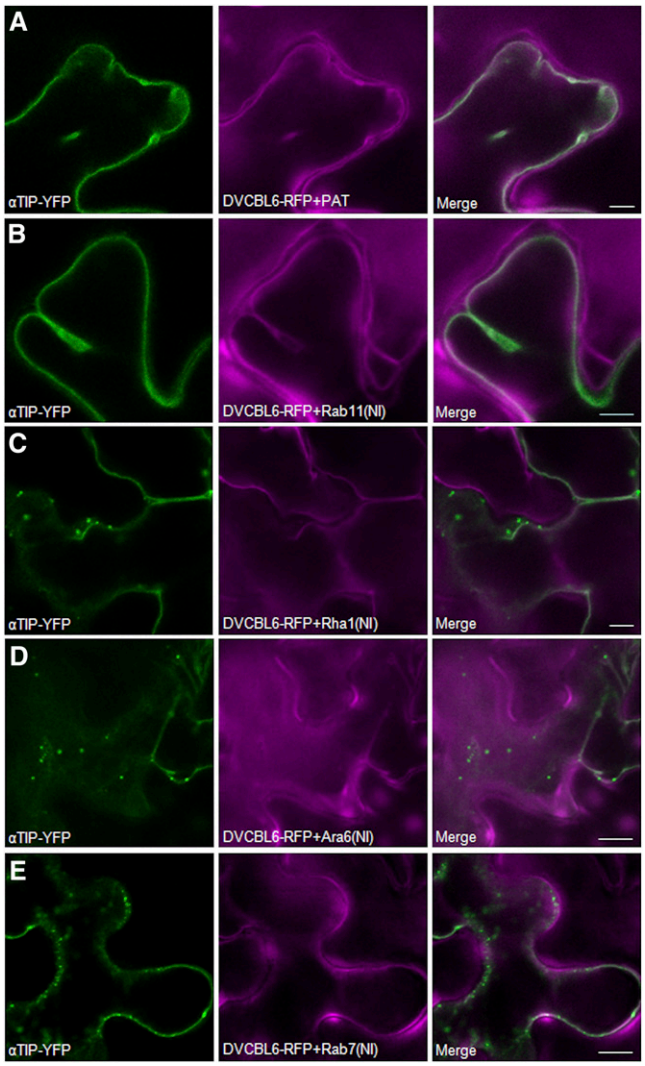

Figure 7. αTIP-YFP but Not CBL6-RFP Trafficking Is Rha1, Ara6, and Rab7 Dependent.

Tobacco leaves were coinfiltrated with *Agrobacterium* strains encoding αTIP-YFP together with the various dual expression vectors for CBL6-RFP, and the various Rab mutants and annotations are as before. Notice that none of the effectors alters the tonoplast localization of CBL6-RFP, while αTIP-YFP is blocked in punctate structures en route to the tonoplast upon coexpression with Rha1(NI) **(C)**, Ara6(NI) **(D)**, or Rab7 (NI) **(E)**. Bars = 10 μm.

Vacuolar Sorting of RFP-CBL6 Is COPII Independent in Contrast with That of Aleu-RFP, GFP-Vam3, and αTIP-YFP

Proteins of the CBL family have been previously reported to be insensitive to a GTP trapped mutant of the GTPase Sar1, suggesting that they exit the ER via a COPII-independent pathway (Batistic et al., 2010). Aleurain is a well known VSR ligand (Ahmed et al., 2000), and it has recently been suggested that VSRs and their ligands may exit the ER via a COPII-independent pathway (Niemes et al., 2010). Tail-anchored proteins such as the SNARE Vam3 are inserted into the membrane at the level of the ER, but the COPII dependency for ER export has never been tested. Finally, αTIP was earlier reported to reach the vacuole in a BFA-insensitive manner (Gomez and Chrispeels, 1993). For these reasons it was important to compare systematically the COPII dependence of CBL6-RFP, Aleu-RFP, GFP-Vam3, and αTIP-YFP with respect to vacuolar sorting.

COPII-mediated ER export can be disrupted by overexpressing Sec12, the exchange factor of the small GTPase Sar1. This results in Sar1 titration, disruption of coat formation, and inhibition of constitutive secretion of soluble proteins (Phillipson et al., 2001). Sec12 overexpression also disrupts ER export sites and causes ER retention of the Golgi marker ST-YFP (daSilva et al., 2004). To test the COPII dependency of the various cargo molecules, two new dual expression plasmids were generated that each encode one of the TR2′-driven Golgi markers ST-YFP or ST-RFP together with the untagged Sec12 gene product under control of the cauliflower mosaic virus 35S promoter. Cells that showed a partial redistribution of the Golgi marker to the ER

were guaranteed to express sufficient levels of the untagged Sec12 gene product to disrupt COPII-mediated ER export.

Tobacco leaves were thus coinfiltrated with an *Agrobacterium* strain encoding CBL6-RFP, Aleurain-RFP, or GFP-vam3 together with the new dual expression vector for ST-YFP and Sec12. In the case of αTIP-YFP, coexpression was performed with the dual vector encoding ST-RFP and Sec12. Figure 8A shows that Sec12 overexpression failed to inhibit trafficking of CBL6-RFP to the vacuolar membrane. When the same cells were imaged at the cell cortex, most of the Golgi marker was retained in the reticular ER, but no CBL6-RFP fluorescence was detected in those structures (Figure 8B). By sharp contrast, Sec12 overexpression caused a dramatic retention of Aleu-RFP in the ER, even when ER redistribution of the Golgi marker ST-YFP was partial and ST-YFP–labeled Golgi bodies were readily observed (Figure 8C). This shows that ER export of Aleu-RFP is COPII dependent in sharp contrast to earlier suggestions (Niemes et al., 2010). Interestingly, ER export of the two vacuolar membrane proteins GFP-Vam3 and αTIP-YFP was also highly sensitive to Sec12 overexpression (Figures 8D and 8E), confirming that they exit the ER in a COPII-dependent manner.

In contrast with the other cargo molecules, we confirm that CBL6-RFP reaches the vacuolar membrane via a COPII-independent pathway as recently proposed (Batistic et al., 2010). Moreover, as CBL6 sorting was not influenced by Rab mutants that affect further transport events in post-Golgi compartments (Figure 7), this route may bypass the secretory pathway all together.

Rab7-Induced Fusion of Post-Golgi Organelles

Although nucleotide-deficient Rab7 interfered with vacuolar delivery of the transmembrane cargo GFP-Vam3, the vacuolar membrane and the Golgi apparatus remained intact under these conditions. However, compared with Rab7(NI)-mediated punctate structures containing αTIP-YFP (Figure 7E), Rab7(NI)-induced GFP-Vam3 retention caused formation of much larger mobile clusters. These are similar in size to the PVC clusters observed upon overexpression of Pep12 (Foresti et al., 2006). For these reasons we wanted to assess markers of plant post-Golgi organelles for their presence in this compartment. The dual expression vector containing the nucleotide-free Rab7(NI) mutant used in previous experiments was reconstructed to replace the TR2′-driven internal Golgi marker ST-YFP by markers for post-Golgi organelles. These included the TGN-marker YFP-Syp61 (Foresti and Denecke, 2008), the PVC marker RFP-VSR2 (Foresti et al., 2010), the vacuolar lumen marker Aleu-RFP (Foresti et al., 2010), or CBL6-RFP as internal standards. Coexpression of these new dual expression vectors with GFP-Vam3 would allow identification of Rab7(NI)-expressing cells via monitoring the red fluorescent internal standards and at the same time test if coexpressed GFP-Vam3 is colocalized in the enlarged clusters with the various post Golgi organelle markers.

When GFP-Vam3 was coexpressed with YFP-Syp61 and Rab7(NI), enlarged structures showed perfect colocalization of the two fluorescent markers (Figure 9A). The results suggest that Rab7(NI) causes either TGN retention of GFP-Vam3 or fusion of the TGN with the PVC to form a supercompartment. This is in

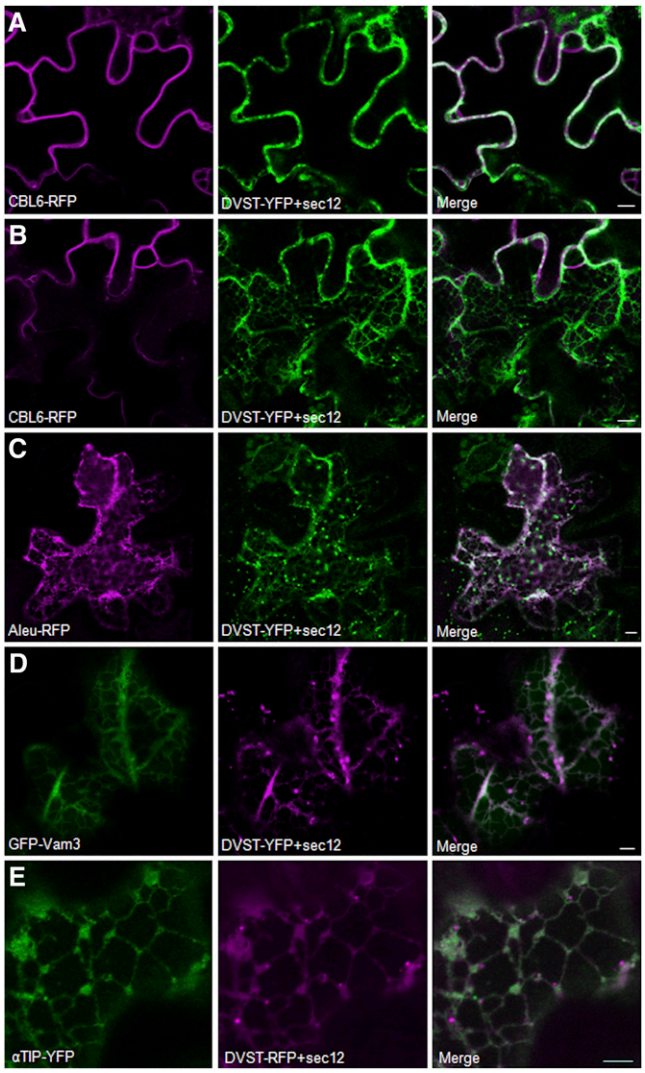

Figure 8. While Aleu-RFP, GFP-Vam3, and αTIP-YFP Exit the ER in COPII Vesicles, CBL6-RFP Trafficking Is sec12 Independent.

This tobacco leaf infiltration experiment was based on an *Agrobacterium* strain harboring a new dual expression vector encoding the Golgi marker ST-YFP (**[A]** to **[D]**) or ST-RFP **(E)** as well as a Sec12 overexpression cassette for inhibition of COPII-mediated ER export. This vector was cotransformed with *Agrobacterium* strains harboring either CBL6-RFP (**[A]** and **[B]**), Aleu-RFP **(C)**, GFP-Vam3 **(D)**, and αTIP-YFP **(E)**. Only cells displaying ER-retained Golgi marker ST-YFP were imaged as they contained inhibitory levels of the Sec12 gene product. **(A)** shows the midsection of a transfected cell in which it is possible to evaluate normal CBL6-RFP staining of the tonoplast. **(B)** shows the cortex of the same cell in **(A)** where it can be noted that CBL6-RFP has not redistributed to the ER, in spite of strong ER retention of the Golgi marker ST-YFP, which served as positive control for Sec12 action. On the contrary, Sec12 overexpression caused redistribution of GFP-Vam3 **(C)**, Aleu-RFP **(D)**, as well as αTIP-YFP **(E)** into the ER. Bars = 10 μm.

contrast with the Golgi marker that remains separate from Rab7 (NI)-induced clusters (Figure 6E). Rab7(NI) clusters also show colocalization of GFP-Vam3 with the PVC marker RFP-VSR2 (Figure 9B) or the vacuolar cargo Aleu-RFP (Figure 9C). This shows that the enlarged clusters contain markers for the TGN, the PVC, as well as soluble and membrane vacuolar markers. By contrast, CBL6-RFP was excluded from the clusters (Figure 9D, arrowheads), and the subcellular distribution of the CBL6-RFP chimera remained normal even under conditions where Rab7(NI) and GFP-Vam3 are coexpressed.

We also recorded time series to document cell viability and organelle motion at the time of imaging (Figure 10; see Supplemental Movies 1 and 2 online). Figure 10A shows that enlarged Rab7(NI)-induced clusters carrying the marker GFP-Vam3 are mobile and move independently from Golgi bodies (see Supplemental Movie 1 online). The latter are well separated from the Rab7(NI) clusters and show normal morphology and mobility. By contrast, the TGN marker YFP-SYP61 is found together with GFP-Vam3 in Rab7(NI)-induced mobile clusters (Figure 10B; see Supplemental Movie 2 online). Identical results as those in Figure 10B were obtained with the RFP-VSR2 and Aleu-RFP in the dual expression vectors (data not shown). A final control was to test if constitutive secretion was affected by Rab7(NI) or the three other nucleotide-free Rab mutants in both expression systems. In protoplasts, constitutive secretion of the model cargo α-amylase was unaffected by the four individual Rab mutants (see Supplemental Figure 3A online). Similar results were obtained in situ with secreted RFP in tobacco leaf epidermis using Rab7(NI) (see Supplemental Figure 3B online) and the other three Rab mutants (data not shown).

The results illustrate that inhibition of vacuolar sorting does not compromise constitutive secretion, confirming earlier results (Pimpl et al., 2003; daSilva et al., 2005; Foresti et al., 2006). More specifically, Rab7(NI)-induced enlarged PVC clusters exclude Golgi and vacuole membranes because these structures remain intact and harbor markers that do not partition into the clusters. Their high directional mobility (see Supplemental Movies 1 and 2 online) shows that clustering/fusion of post-Golgi/prevacuolar compartments is not due to cell mortality or unspecific aggregation. Finally, the work indicates that CBL6-RFP may reach the tonoplast via a noncanonical mechanism that may either bypass the organelles of the secretory pathway completely or follow an as yet unknown route from the plant ER.

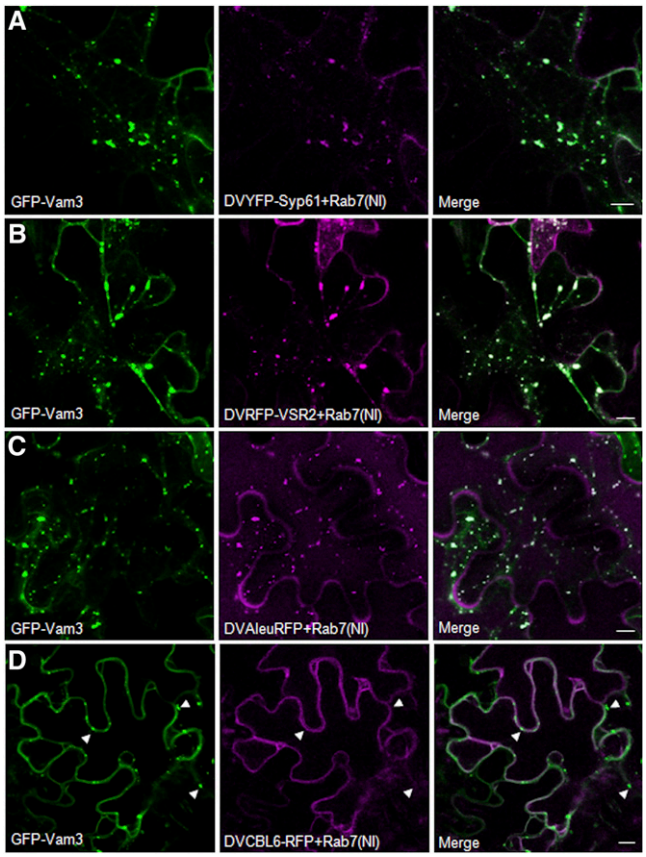

Figure 9. The Mobile Clusters Contain Markers for the TGN, the PVC, and the Vacuole but Not CBL6-RFP.

Tobacco leaves were infiltrated with an *Agrobacterium* strain encoding GFP-Vam3 together with new double vectors containing Rab7(NI) as effector and either the TGN marker YFP-SYP61 **(A)**, the PVC marker RFP-VSR2 **(B)**, the soluble vacuolar marker Aleu-RFP **(C)**, or the tonoplast-localized CBL6-RFP **(D)**. YFP-SYP61 **(A)** and RFP-VSR2 **(B)** redistribute into the same mobile clusters in the presence of GFP-Vam3 and Rab7(NI). The soluble vacuolar marker Aleu-RFP is also observed in these putative TGN-PVC supercompartments **(C)**. GFP-Vam3 is trapped in the clusters in the presence of Rab7(NI) but these exclude CBL6-RFP (white arrowheads) as the CBL6 fusion still reaches the vacuolar membrane **(D)**. Bars = 10 μm.

DISCUSSION

Involvement of Rab11 and Rab7 in Transport to the Lytic Vacuole

With the aim to identify a set of transport inhibitors to characterize individual transport steps along the biosynthetic route to the vacuoles, a range of NI mutants of Golgi and post-Golgi Rab GTPases was tested in a quantitative screen for induced secretion of soluble vacuolar cargo. Members of the Rab6 and Rab8 group did not influence vacuolar sorting, suggesting that they may play a role in constitutive secretion or recycling. By contrast, a member of the plant Rab11 GTPase, a representative member of the canonical Rab5 GTPase (Rha1), the plant-specific Rab5 GTPase (Ara6), and a member of the Rab7 GTPase tested positive in this assay (Figure 1). While the role of both Rab5 family members in vacuolar sorting has been reported previously (Sohn et al., 2003; Bolte et al., 2004; Kotzer et al., 2004; Lee et al., 2004), our work introduces Rab11 and Rab7 as additional tools to examine vacuolar transport steps before and after Rab5-mediated processes. Soluble vacuolar cargo can be detected in post-Golgi structures in transit to the vacuoles under control conditions. Rab11(NI) causes a reduction of these trafficking intermediates (cf. Figures 4A and 4B), while the two Rab5(NI) mutants [Rha1(NI) and Ara6(NI)] and in particular Rab7(NI) caused an increase (Figures 4C to 4E). This suggests a sequential action of Rab11, Rab5, and Rab7 members in transport to the plant vacuole.

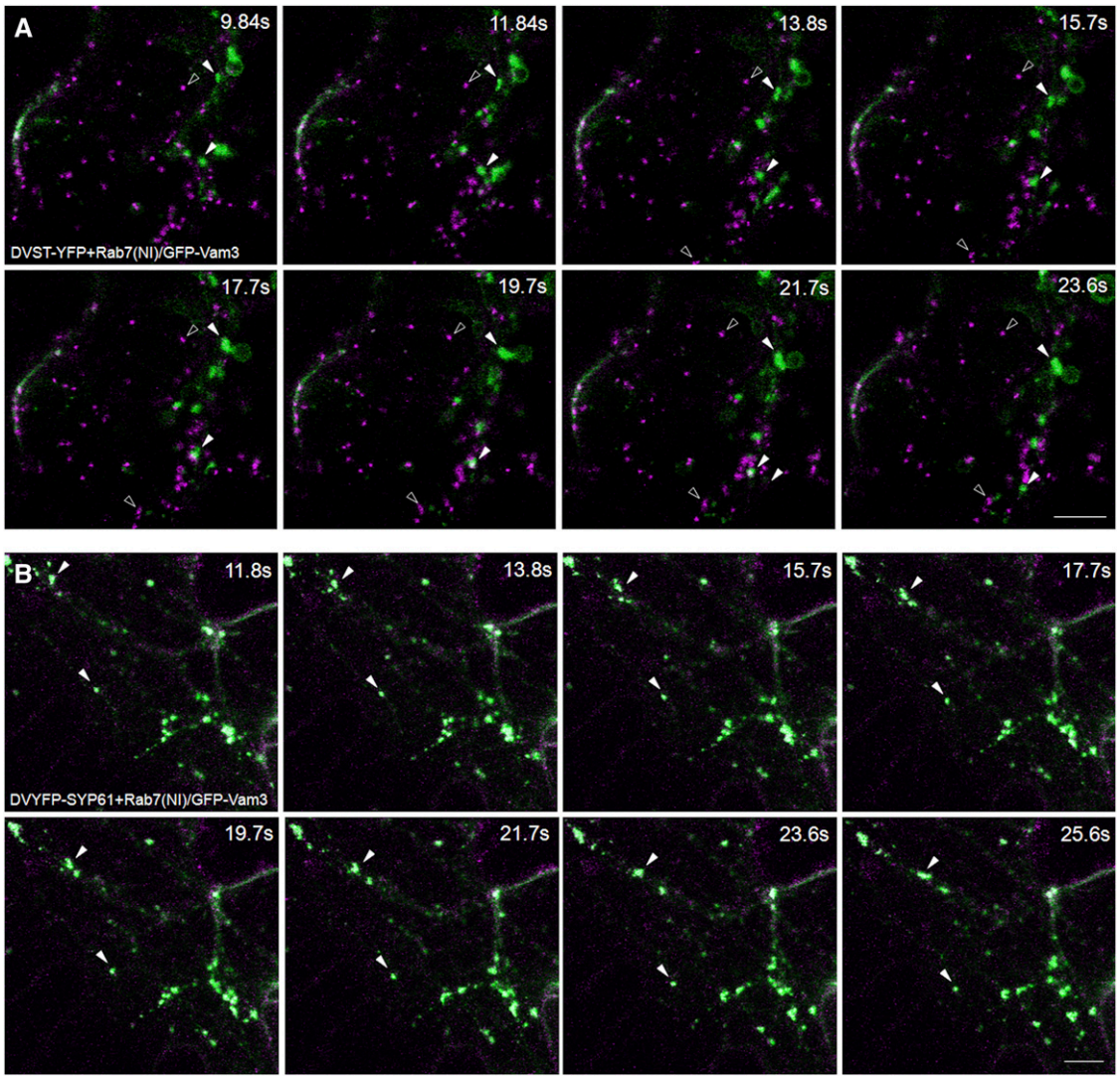

Figure 10. Mobility of the TGN-PVC Clusters Is Not Compromised.

(A) Selected frames from a time series recorded from a leaf epidermal cell coexpressing the dual expression vector harboring the Golgi marker ST-YFP and Rab7(NI) along with the GFP-Vam3 chimera. White arrowheads follow the movement of the mobile clusters (green) in the various frames, while black arrowheads follow the movement of the separate Golgi bodies (purple).

(B) Selected frames from a time series recorded from a leaf epidermal cell coexpressing the dual expression vector harboring YFP-SYP61 and Rab7(NI) together with the GFP-Vam3 chimera. Arrowheads indicate the movement of the clusters that contain both the TGN and tonoplast markers (pale green). Bars = 10 μm.

Members of the Rab11 family in plants have been implicated in biosynthetic trafficking to the plasma membrane and cell plate formation (Chow et al., 2008). Moreover, Rab11 has been implicated in root hair cell growth (Preuss et al., 2004, 2006) and pollen tube growth (Szumlanski and Nielsen, 2009) in agreement with a possible role in polarized secretion of cell wall components. However, no evidence for a role on the vacuolar branch of the secretory pathway had been previously proposed. Vacuolar and secretory cargo have been suggested to deviate at the level of the TGN (Dettmer et al., 2006; Toyooka et al., 2009; Viotti et al., 2010). Electron tomography of the TGN suggests the presence of microdomains on the TGN either covered with clathrin or uncoated (Staehelin and Kang, 2008). Since the VSR BP80 was isolated from clathrin-coated vesicles (Kirsch et al., 1994), it can be speculated that clathrin-coated domains may be involved in vacuolar sorting, while uncoated domains may possibly be implicated in secretory vesicle budding. Rab11 may play a role in maintaining the microdomain structure required to maintain efficient vacuolar sorting.

It is also possible that plant Rab11 may play a primary role in endocytic recycling back to the plasma membrane as is the case for its mammalian homolog (Ullrich et al., 1996). Rab11

knockout–induced defects in cell plate deposition or tip growth of pollen tubes and root hairs (Preuss et al., 2004, 2006; Szumlanski and Nielsen, 2009) may thus be indirect secondary effects. If a significant portion of VSRs cycle via the plasma membrane (Foresti et al., 2010; Saint-Jean et al., 2010), interference with Rab11-mediated recycling could compromise VSR endocytosis and cause partial mis-sorting of cargo to the apoplast. This may explain the Rab11(NI)-mediated reduction of post-Golgi structures labeled with soluble cargo in transit to the vacuole (Figure 4B). It would also explain the weaker effect of Rab11(NI) on the trafficking of vacuolar cargo compared with Rab5(NI) and Rab7(NI) (Figures 1B and 3B) as the majority of receptors may reach the PVC without passing via the plasma membrane. Since the Rab11 family is unusually large in plants and functional differentiation has been suggested for some of its members (Chow et al., 2008), further work must be performed with other Rab11 members and can now include the simple vacuolar transport assay in addition to localization studies.

While Rab11 is localized to the TGN upstream from the PVC, Rab7 was found to reside on the tonoplast (Nahm et al., 2003) and would therefore be expected to act at the very last step of the pathway. By analogy to the yeast homolog Ypt7 (Haas et al., 1995), plant Rab7 could facilitate PVC fusion with the vacuolar membrane. Rab7 overexpression was shown to induce salt and osmotic stress tolerance in *Arabidopsis* (Mazel et al., 2004), but its role in vacuolar transport was not addressed. Here, it is demonstrated that Rab7(NI) causes a similar induced secretion of vacuolar cargo as seen for the Rab5 mutants Rha1(NI) and Ara6(NI) (Figures 1 to 3). In addition, Rab7(NI) causes a drastic accumulation of post-Golgi transport intermediates harboring vacuolar cargo in transit (Figure 4E). This was much more pronounced than that observed for the Rab5 mutants Rha1(NI) and Ara6(NI) (Figures 4C and 4D), which may act at an earlier step in the pathway.

Increased levels of vacuolar cargo in transit would be consistent with a role of Rab7 in PVC to vacuole fusion. However, it was unexpected that accumulation in the PVC would lead to secretion. Constitutive secretion may occur from the Golgi stack or the TGN, but in the first instance it is hard to imagine how secretion could still occur at the level of the PVC. However, there is also evidence for the existence of secretory routes that traffic through the late endosome in yeast and mammals (Harsay and Schekman, 2002; De Matteis and Luini, 2008). In hematopoietic cells, late endosomes and lysosomes have a role in exocytosis and can fuse directly with the PM (Théry et al., 2002). Moreover, some viruses were shown to hijack the secretory pathway and cause fusion of late endosomes to the PM for the release of newly synthesized viral particles (Pelchen-Matthews et al., 2004). There is also evidence in plants suggesting that under specific physiological conditions, multivesicular bodies could fuse with the plasma membrane and thus release internal vesicles as the so-called exosomes or paramural vesicles that accumulate between the plasma membrane and the cell wall (An et al., 2006, 2007). Future work will have to reveal if pathogens may interfere with Rab7-mediated trafficking to mediate this type of mis-sorting and if different members of the plant Rab7 family carry out specialized functions.

ssVSS and ctVSS Cargo Follow the Same Route to the Vacuole in Plant Cells

Evidence pointing toward the existence of different pathways leading to the vacuole in plant cells came from reports using a single effector to interfere with vacuolar sorting (Matsuoka et al., 1995; Bolte et al., 2004; Zouhar et al., 2009). Here, the trafficking of α-amylase fusions bearing either ssVSS or ctVSS was monitored in response to increased dosage of the four different transport inhibitors identified in the screen (Figure 1B). Evidence for two distinct pathways would be given if one inhibitor specifically affected the sorting of one class but not the other and another inhibitor showed the opposite specificity.

Using barley α-amylase as quantitative transport cargo, we tested the ssVSS from sweet potato sporamin (Kirsch et al., 1994; Matsuoka and Nakamura, 1999) at the C terminus of the enzyme (amy-spo) as well as barley aleurain propeptide sequence (Di Sansebastiano et al., 2001) at the N terminus of α-amylase (Aleu-amy) for putative trafficking to the lytic vacuole (Figures 2A and 2B). To represent ctVSSs, we used the propeptides of chitinase (Neuhaus et al., 1991) and Brazil nut 2S storage albumin (Saalbach et al., 1996) for C-terminal fusions with the enzyme (amy-chi and amy-BN2SA) and tested putative sorting to the storage vacuole (Figures 2C and 2D).

The results of the dose–response analysis failed to reveal any meaningful differences in the specificity for the two classes of cargo molecules and certainly did not reveal opposite specificities. The only noticeable difference was a lower vacuolar sorting fidelity compared with our model cargo amy-spo and a higher maximum induced secretion, which was ~2× higher in all other cases (Figure 2). This minor discrepancy could easily be explained by the fact that amy-spo is a stronger ligand for the same VSR.

The work shows that four different NI mutants of Rab GTPases acting at different stages of the pathway interfere with ssVSS- and ctVSS cargo trafficking indiscriminately. In situ studies in the leaf epidermis system also failed to reveal differences in the vacuolar transport route of ssVSS and ctVSS cargo, except that RFP-chi was slowly exported from the ER compared with Aleu-RFP, which rapidly reaches post-Golgi structures and the vacuoles (cf. Figures 3 and 4 with 5). Inhibition of vacuolar sorting by NI mutants of GTPases revealed accumulation in punctate post-Golgi structures of both cargo molecules when the two Rab5 mutants were coexpressed and stronger prevacuolar retention in the case of Rab7(NI). By contrast, Rab11(NI) reduced the detection of cargo in post Golgi structures. Both types of cargo behaved in the same manner.

The combined results are in agreement with VSR knockdown experiments in *Arabidopsis* (Craddock et al., 2008) and the fact that both ssVSS and ctVSS cargo were shown to traffic through the same PVC (Miao et al., 2008). We were unable to support earlier reports on differential inhibition (Bassham et al., 2000; Sanderfoot et al., 2001; Bolte et al., 2004; Sanmartín et al., 2007; Zouhar et al., 2010).

Evidence for Multiple Transport Mechanisms for the Targeting of Membrane-Spanning Vacuolar Cargo

Due to their different topologies, the sorting of transmembrane and soluble proteins must occur via completely different sorting

mechanisms, even if they share the same transport organelles. Soluble proteins occupy the lumen of organelles and vesicles and either passively diffuse into the membrane carriers (Denecke et al., 1990) or rely on the binding to membrane-spanning receptors if they carry active sorting signals. On the other hand, transmembrane proteins span the limiting membrane of organelles and vesicles and thus bear motifs in their cytoplasmic domains for direct interaction with cytosolic components that shape and deliver transport carriers.

In this study, three classes of membrane spanning vacuolar cargo were compared with the soluble vacuolar reporters, and the results show that they display different transport sensitivity in response to coexpression of the various Rab GTPase mutants. Tonoplast targeting of an αTIP-YFP fusion protein was clearly sensitive to NI mutants of the two Rab5 GTPases and Rab7 (Figures 7C to 7E). This was also observed for soluble vacuolar cargo bearing either ssVSS (Figures 4C to 4E) or ctVSS signals (Figures 5C to 5E). Clear accumulation in punctate structures was most obvious in the case of Rab7(NI) and undetectable for Rab11 (NI). The same was observed for soluble cargo, except for a mild induction of secretion of the α-amylase fusion proteins (Figure 2), due to higher sensitivity and quantification by the protoplast transport assay. In conclusion, αTIP-YFP is transported in a similar manner as soluble cargo regardless of the VSS.

Tonoplast targeting of tail-anchored GFP-Vam3 was insensitive to NI mutants of Rab11 Rab5 (Figures 6B to 6D). Only Rab7 (NI) trapped the SNARE fusion in an enlarged post-Golgi structure that contained markers for the PVC, the TGN, and soluble vacuolar cargo but not the Golgi marker (Figure 6E). The results suggest that the early transport steps controlling Vam3 delivery to vacuoles differ from those of soluble cargo and α-TIP, although both types of cargo may merge at the level of the PVC prior to a common Rab7-mediated PVC-to-vacuole fusion event. In addition, the differential sensitivity of Vam3 to Rab5 and Rab7 mutants provides the strongest evidence for functional differentiation between the two classes of Rab GTPases.

Any branching in the pathway would have to be placed from the level of the Golgi onwards because ER export of Aleu-RFP, αTIP-YFP, and GFP-Vam3 was sensitive to Sec12 overdose and thus COPII dependent (Figures 8C and 8D). Interesting parallels can be drawn with results obtained in the yeast *Saccharomyces cerevisiae*, where Golgi-mediated sorting of the vacuolar t-SNARE Vam3 and the soluble cargo carboxypeptidase Y depend on different machinery (Cowles et al., 1997). Results presented in this study present a first step toward elucidating the true complexity of post-Golgi trafficking in plants. It will also be interesting to analyze the recently characterized two-pore K^+ channels TPKa and TPKb that show differential subcellular localization in rice (*Oryza sativa*) protoplasts and test their dependence on the portfolio of inhibitors used in this study (Isayenkov et al., 2011).

The CBL6-RFP chimera represents a totally different case study because its arrival at the vacuolar membrane was insensitive to any of the transport inhibitors used (Figures 7, 8A, and 8B). The results suggest that CBL6 segregates from Vam3 and soluble cargo at the ER export step as it is not COPII dependent. This is in agreement with earlier studies based on the use of a GTP-trapped form of the small GTPase Sar1 as a COPII transport inhibitor (Batistic et al., 2010). Moreover, the results with the mutant Rab GTPases suggest that the pathway does not merge at later stages.

On the basis of the results obtained, the most probable scenario is that CBL6 may not enter the secretory pathway at all and could insert directly into the vacuolar membrane after synthesis in the cytosol. However, the CBL6 sequence bears no consensus sites for lipid anchoring and instead contains an N-terminal hydrophobic region (Batistic and Kudla, 2009). This region lacks the typical -1-3 region for signal peptide processing (von Heijne and Gavel, 1988) and appears to be a noncleavable transmembrane domain, although the mechanism of insertion remains to be established. Further work will have to be performed to confirm this hypothesis and to characterize the pathway.

Fusion of Post-Golgi Compartments

Overexpression of Rab7(NI) caused two interesting effects that deserve to be mentioned specifically. First, it was noticeable that soluble cargo accumulates to a greater extent in post-Golgi structures compared with coexpression experiments with the two Rab5 GTPase mutants (cf. Figure 4E with 4C and 4D). This effect appeared to be exacerbated when GFP-Vam3 was coexpressed with Rab7(NI), causing clustering/enlargement of post Golgi compartments (Figures 9 and 10). These structures are larger than those observed when Rab7(NI) was coexpressed with the soluble markers Aleu-RFP and RFP-chi (Figures 4 and 5) or the membrane cargo αTIP-YFP (Figure 7). They also show similarity to the PVC clusters observed upon Pep12 overexpression (Foresti et al., 2006). Given the fact that Vam3 and Pep12 have been proposed to display interchangeable functions (Uemura et al., 2010), it is possible that Vam3 retention in the PVC leads to a Pep12 overproduction phenotype.

Further analysis with organelle markers revealed that Rab7 (NI)-induced GFP-Vam3 clusters contained also the TGN marker YFP-SYP61 (Figure 9A), the PVC marker RFP-VSR2 (Figure 9B), and the soluble vacuolar cargo Aleu-RFP (Figure 9C). These results suggest that a TGN-PVC supercompartment is formed that strictly excludes the alternative vacuolar cargo CBL6-RFP (Figure 9D) and the Golgi marker ST-YFP (Figure 6E). However, the cells are capable of normal constitutive secretion (see Supplemental Figure 3 online), they show normal cytoplasmic streaming, and the enlarged clusters retain high directional mobility (Figure 10; see Supplemental Movies 1 and 2 online) and cannot be regarded as unspecific terminal aggregates.

Colocalization of TGN with PVC markers in enlarged structures has also been observed in response to the drug Wortmannin (Wang et al., 2009), which was earlier shown to inhibit recycling of plant VSRs (daSilva et al., 2005). Wortmannin-induced enlargement was accompanied by vacuolation, whereas the Rab7(NI)-induced structures do not appear to be vacuolated.

It is curious to note that a late transport defect should lead to fusion of the PVC with an earlier compartment, but precedence for such a scenario in the early secretory pathway arose two decades ago from observations with the drug BFA, which causes fusion of entire Golgi cisternae with the ER (Lippincott-Schwartz et al., 1989). It was later shown that the drug causes titration of the GTPase ARF1 in an abortive complex with its exchange

factor, leading to inhibition of retrograde COPI-mediated Golgi-to-ER transport (Peyroche et al., 1999). In plant cells expressing BFA-resistant ARF1 exchange factors, this early transport defect is replaced by a later transport defect surrounding the TGN (Geldner et al., 2003; Geldner, 2004; Lam et al., 2009). Further work will have to be performed to study the conditions promoting post-Golgi organelle fusion in plants and to identify common denominators that may shed further light on this phenomenon.

METHODS

Recombinant DNA Plasmids Encoding Cargo Molecules

A schematic representation of plasmids used in this study is given in Supplemental Figure 4 online. Previously described plasmids include those encoding the soluble vacuolar cargo amy-spo (Pimpl et al., 2003; daSilva et al., 2005), α-amy (Phillipson et al., 2001), Aleu-RFP (Foresti et al., 2010), the membrane cargo GFP-Vam3 (Foresti et al., 2006), and αTIP-YFP (Hunter et al., 2007). To generate the alternative vacuolar cargo construct with the sorting signal of tobacco (*Nicotiana tabacum*) chitinase, pAmy (Phillipson et al., 2001) was digested with *Bgl*II and *Hin*dIII to generate the vector. pAmy was also digested with *Xba*I and *Hin*dIII to isolate the 3′nos fragment, and the two oligonucleotides NtChis and NtChias (see Supplemental Figure 5A online) were annealed to generate a *Bgl*II-*Xba*I compatible fragment. Both fragments were ligated together into the above-described vector to yield pAmy-chi. To generate a vacuolar cargo construct with the sorting signal of the Brazil nut storage albumin, the same procedure was used except for the annealed fragment, which was generated using oligonucleotides BN2SAs and BN2SAas (see Supplemental Figure 5A online) to yield pAmy-BN2SA. To generate an α-amylase fusion bearing the barley (*Hordeum vulgare*) aleurain propeptide sequence (Di Sansebastiano et al., 2001), pAleu-RFP (Foresti et al., 2010) was digested with *Nhe*I and *Bam*HI and deposphorylated. A compatible α-amylase fragment was generated by amplifying pAMY (Phillipson et al., 2001) with the primers amys and 3′nosas (see Supplemental Figure 5A online), gel purified, and ligated into the previously generated vector.

To generate a secreted variant of RFP, pRFP-VSR2(L615A) (Foresti et al., 2010) was digested with *Bgl*II and *Hin*dIII and deposphorylated. pAMY (Phillipson et al., 2001) was also digested with *Bgl*II and *Hin*dIII, and the obtained fragment was gel purified and ligated into the previously generated vector, yielding psecRFP. To generate a fusion between CBL6 and RFP, pAleu-RFP was digested with *Cla*I and *Nhe*I and dephosphorylated. The CBL6 coding region was amplified using primers CBL6s and CBL6as (see Supplemental Figure 5A online), digested with *Cla*I and *Nhe*I, and gel purified. Vector and fragment were ligated to yield pCBL6-RFP. To generate a fusion between RFP and the ctVSS from tobacco chitinase, psecRFP was amplified with an oligonucleotide annealing to the 35S promoter region (35Ss) and RFPChias (see Supplemental Figure 5A online). The resulting PCR fragment was digested with *Cla*I and *Xba*I, gel purified, and ligated into pVENUS-Rha1 (Foresti et al., 2010) that had been previously digested with *Cla*I and *Xba*I and deposhorylated.

Cloning and Mutagenesis of Rab GTPase Coding Regions

Rab GTPases were cloned by PCR from first-strand cDNA from 5-d-old seedlings prepared as described previously (Pimpl et al., 2003). Rab8 and Rab11 coding regions were amplified to yield *Nco*I-*Bam*HI flanked coding regions with sense and antisense primers indicated in Supplemental Figure 5B online. After digestion and gel purification, these were ligated into pAmy (Phillipson et al., 2001) previously digested with *Nco*I-*Bam*HI and dephosphorylated to yield pRab8 and pRab11. The Rab5 members Rha1 and Ara6 as well as Rab6 and Rab7 coding regions were amplified to yield *Nco*I-*Xba*I flanked coding regions with sense and antisense primers indicated in Supplemental Figure 5B online. After digestion and gel purification, these were ligated into pAmy-HDEL (Phillipson et al., 2001) previously digested with *Nco*I-*Xba*I and dephosphorylated to yield pRha1, pAra6, pRab6, and pRab7.

Mutagenesis of all Rabs to generate the NI mutants was done via the QuickChange method (Stratagene) using pairs of oligonucleotides encoding for the mutated triplet and 15 bases extending on either side of the mutated codon. All mutagenesis primers for each specific Rab GTPase are shown in Supplemental Figure 5C online. All resulting clones were verified by sequencing.

Dual Expression Vectors

Several steps were required to generate the dual expression vector using primers described in Supplemental Figure 5D online. A TR2′ promoter fusion with the Golgi marker ST-YFP was generated by assembly PCR using first the primer pair TR2EcoRIs with TRSTYas and the plasmid pOP443 (Velten et al., 1984) as template, resulting in a modified TR2′ promoter fragment. The primer pair TRSTYs with STYas and plasmid pLL4 (daSilva et al., 2005) as template were used to generate a modified ST-YFP fragment. The two overlapping fragments were subsequently subjected to 10 PCR cycles for self-priming, followed by further PCR amplification using the primer pair TR2EcoRIs with STYas to yield the assembled TR2′:ST-YFP fragment. This was trimmed with *Eco*RI and *Xba*I and gel purified.

PCR assembly of the 3′ocs:35Spromoter fragment was performed with primer pair 3ocsXba1s with 3ocs35sas and plasmid pDE1001 (Denecke et al., 1992) as template to generate a modified 3′ocs sequence. The primer pair 3ocs35ss with amyas and plasmid pAmy as template (Phillipson et al., 2001) resulted in the amplification of a modified 35S promoter fragment. The two overlapping amplification products were subsequently subjected to 10 self-priming PCR cycles to generate an assembled fusion, followed by further PCR amplification using the primer pair 3ocsXba1s with amyas to yield the assembled 3′ocs:35Spromoter fragment. This was ultimately trimmed with *Xba*I and *Nco*I and gel purified.

To generate the double expression vector, plasmid pDE317 was digested with *Eco*RI and *Nco*I to remove the 35S promoter in front of the PAT-3′nos region (Denecke et al., 1992) followed by dephosphorylation. The two assembled and trimmed DNA fragments described above were ligated into this vector to generate plasmid pFB62 carrying the dual expression cassette TR2-ST-YFP-3′ocs/35S-PAT-3′nos. This plasmid was used as starting point for all subsequent double expression vector construction.

The PAT coding region in pFB62 was removed with an *Nco*I-*Bam*HI digestion followed by dephosphorylation. All Rab GTPase coding regions and mutations thereof were isolated as compatible *Nco*I-*Bam*HI fragments and ligated into pFB999. These plasmids were used for quantitative transient expression experiments in conjunction with pAMY derivatives. For tobacco leaf infiltrations, the entire double expression cassettes were cloned between the *Eco*RI and *Hin*dIII sites of pDE1001 (Denecke et al., 1992) using standard recombinant DNA procedures, yielding pTFB62 and derivatives containing Rab coding regions.

The Golgi marker ST-YFP was replaced by the TGN marker YFP-SYP61 (Foresti and Denecke, 2008) by digesting pTFB62 with *Eco*RI and *Xba*I and dephosphorylation. pTFB62 was also digested with *Cla*I, followed by Klenow treatment, and subsequent *Eco*RI digestion and gel purification. The YFP-SYP61 fragment was obtained by digesting pOF61 with *Nco*I, followed by Klenow treatment, subsequent *Xba*I digestion, and gel purification. The two fragments were then jointly ligated into pTFB62 to yield pTFB73 carrying the dual expression cassette TR2-YFPSYP61-3′ocs/35S-PAT-3′nos. pTFB62 was treated with *Xba*I, Klenow, and *Cla*I, followed by dephosphorylation to generate a vector. CBL6-RFP was processed with *Bam*HI, Klenow, and *Cla*I, gel purified, and ligated in the above-described vector, yielding pTFB86, carrying the dual expression cassette

TR2-CBL6-RFP-3′ocs/35S-PAT-3′nos. pTFB86 was digested with *Cla*I and *Pvu*II and dephosphorylated. pAleu-RFP was digested with *Cla*I and *Pvu*II, gel purified, and ligated in the above-described vector, yielding pFB90. pTFB62 was treated with *Xba*I, Klenow, and *Cla*I, and dephosphorylated. RFP-VSR2 was obtained by treating pOF100 (Foresti et al., 2010) with *Bam*HI, Klenow, and *Cla*I, followed by gel purification, for ligation into the vector. This resulted in plasmid pTFB97 carrying the dual expression cassette TR2-RFP-VSR2-3′ocs/35S-PAT-3′nos. In all the dual expression vectors, replacement of PAT by the various Rabs was performed as for pFB62. The dual expression vector harboring the Golgi marker ST-YFP and the Sec12 overexpression cassette was built by replacing PAT in pTFB62 by a *Nco*I-*Bam*HI fragment derived from pSec12 (Phillipson et al., 2001).

To assess cotransformation and coexpression fidelity on a single-cell level, a dual color expression vector was constructed as follows: pTFB86 was digested with *Nco*I and *Hin*dIII, followed by dephosphorylation. pOF44 (Foresti et al., 2006) was digested with *Nco*I and *Hin*dIII, followed by gel purification of the YFP-SYP121-3′nos fragment, which was subsequently ligated into pTFB86, yielding pRainbow (TR2-CBL6-RFP-3′ocs/35S-YFP-SYP121-3′nos).

Transient Expression in Tobacco Protoplasts

N. tabacum cv Petit Havana SR1 (Maliga et al., 1973) was grown in Murashige and Skoog medium (Murashige and Skoog, 1962) supplemented with 2% Suc in a controlled room at 22°C with a 16-h daylength at a light irradiance of 200 μE m^2 s. Tobacco leaf protoplasts were prepared, electroporated, and harvested following the previously described protocol (Hadlington and Denecke, 2000). Concentrations of plasmids are indicated in the figures and legends.

α-Amylase Assay Procedure

Tobacco protoplasts were incubated for 24 h after electroporation in the dark. Cells and medium were harvested according to the well-established procedure described by Foresti et al. (2006). A sample of culture medium without cells was diluted 1:1 with α-amylase extraction buffer for direct enzymatic analysis. Total cells were recovered as a compact pellet after washing with 250 mM NaCl, and cells were extracted in a final volume (α-amylase extraction buffer + cells) of 500 μL by sonication and centrifugation as described (Foresti et al., 2006). Enzymatic α-amylase assays were performed with the Megazyme substrate (R-CAAR4) according to the manufacturer's instructions and downscaling to microtiter plates as described earlier (Foresti et al., 2006). Absorbances were read at λ = 405 nm against a blank consisting of either medium or cell extracts from mock-transformed protoplasts. All values are provided as differences in optical density (ΔOD) between test samples and blanks, divided by the time in minutes of incubation time and the volume of the extracts in microliters, corrected for dilution of the medium and concentration of cell extracts relative to the original cell suspension, and multiplied by 1000 to obtain ΔOD/min/mL suspension. The SI is the ratio of activity in the medium to that of the cells; the total activity is the sum of the activities in the medium and cells. A detailed procedure has been published previously (Foresti et al., 2006).

Extraction of Protein and Immunoblot Analysis

Protoplast pellets obtained from the harvesting were extracted in 100 μL total volume of phaseolin extraction buffer (daSilva et al., 2005). The extract was then centrifuged at maximum speed for 10 min and the supernatant recovered, diluted 1:1 with sample buffer, and loaded on an SDS-PAGE gel. Protein gel blots and immunodetection were performed as previously described by Pimpl et al. (2006) using an anti-GFP rabbit polyclonal antiserum (Invitrogen).

Cotransfection Practice Using Dual Expression Vectors

For transient expression in tobacco leaf protoplasts, all pFB62-based dual expression vectors were first tested individually by monitoring expression levels of the internal Golgi marker ST-YFP via immunoblotting to normalize transfection efficiencies. Under these conditions, the effect of different Rab GTPases and derived mutants could be compared in a quantitative and reproducible manner. Cotransfection of plasmids encoding the soluble vacuolar cargo molecules derived from barley α-amylase with the dual vectors were tested again for ST-YFP expression as additional quality control. Differences in the effect of RabGTPases expressed from the same plasmid could thus be attributed to the nature of the GTPases themselves rather than variance in transfection efficiency.

Tobacco Leaf Infiltration Procedure and Confocal Laser Scanning Microscopy

Soil-grown *N. tabacum* cv Petit Havana SR1 (Maliga et al., 1973) were infiltrated with *Agrobacterium tumefaciens* cultures (OD = 0.1) of strains harboring the desired plasmids (Sparkes et al., 2006). Infiltrated tobacco leaves were used as starting material for confocal laser microscopy analysis. Imaging of transfected cells was performed early after infiltration and restricted to cells expressing well below the steady state levels to avoid overexpression artifacts. Typically, 24 to 48 h after infiltration, a square of around 0.5 $\times$ 0.5cm was cut from the infiltrated area and mounted on a glass slide, with the lower epidermis facing up the cover glass (22 $\times$ 50 mm, N. 0). Confocal imaging was performed using an upright Zeiss LSM 510 META laser scanning microscope with a Plan-Neofluar $\times$40/1.3 oil differential interference contrast objective. When GFP and YFP were coexpressed, samples were excited with an argon ion laser at the wavelength of 458 nm for GFP and 514 nm for YFP. Fluorescence was detected with a 545-nm dichroic beam splitter and a 480- to 520-nm band-pass filter for GFP and 565 to 615 nm for YFP. When GFP or YFP were coexpressed with RFP, samples were excited with an argon ion laser at the wavelength of 488 nm for GFP or YFP and 543 nm for RFP. Fluorescence was detected with a 545-nm dichroic beam splitter and a 500- to 530-nm band-pass filter for GFP or YFP and 565 to 615 nm for RFP. Postacquisition image processing was performed with LSM 5 image browser (Zeiss) and ImageJ (http://rsb.info.gov/ij/). For all experiments, normal organelle mobility was a prerequisite for further analysis, and fluorescence levels 10- to 20-fold below the steady state levels were found to be ideal for in vivo analysis. Cells with fluorescence levels closer to steady state levels or with static organelles showing merely Brownian motion were not imaged.

Cotransformation Practice for in Situ Expression Using Dual Expression Vectors

Unlike experiments with protoplast populations in which samples are averages of many cells, in situ fluorescent imaging is performed on individual cells displaying variable levels of expression and coexpression. The dual expression vectors derived from pTFB62 for *Agrobacterium*-mediated leaf transformation were used to restrict analysis to only those cells expressing the internal marker as well as the cargo molecule to be influenced. Expression of the internal marker guarantees expression of the GTPase as effector as it is encoded by the same T-DNA. Moreover, using a constant laser output and detector gain, cells could be selected that express comparable levels of internal marker and, thus, GTPase for comparisons. Under these conditions, differences observed in the effect of various GTPases could thus be attributed to the nature of the GTPases, rather than coexpression efficiency.

In Situ Quantification of Aleu-RFP and RFP-Chi in Transit through Post-Golgi Compartments

For colocalization studies of punctate structures that could not be distinguished morphologically and to quantify levels of Aleu-RFP and RFP-chi in transit through post-Golgi organelles relative to the internal marker, we used the PSC colocalization plug-in of Image J (French et al., 2008) to calculate colocalization and to produce scatterplots. A minimum of 20 cells or at least 400 independent punctate were manually masked using the "selection brush" tool as introduced earlier (French et al., 2008). To produce scatterplots with the "analyze" tool, a threshold level of 10 was defined as pixel noise and excluded from statistical analysis. The total intensity of the green and red colors in the resulting scatterplots was measured to provide a red-green ratio, representing Aleu-RFP and RFP-chi in transit through post Golgi compartments relative to the fluorescence of the internal Golgi marker (Green).

Accession Numbers

Sequence data from this article can be found in the GenBank/EMBL databases under the following accession numbers: CBL6 (At4g16350), Rab6 (At2g44610), Rab8 (At5g03502), Rab11 (At1g09630), Rha1 (At5g45130), Ara6 (At3g54840), and Rab7 (At3g16100).

Supplemental Data

The following materials are available in the online version of this article.

Supplemental Figure 1. Cotransformation Efficiency of Two Different Genes from a Single T-DNA Region.

Supplemental Figure 2. Separation of Plasma Membrane from Tonoplast.

Supplemental Figure 3. Rab NI Mutants Do Not Impair Constitutive Secretion.

Supplemental Figure 4. Schematic Drawings of Recombinant Genes Used in This Study.

Supplemental Figure 5. Oligonucleotides Used in This Study.

Supplemental Movie 1. Original Video Data to Figure 10A.

Supplemental Movie 2. Original Video Data to Figure 10B.

ACKNOWLEDGMENTS

We thank James Blaza (Medical Research Council, Cambridge, UK) for constructing the dual expression vector harboring ST-YFP and Sec12 as part of his internship. We also thank Lorenzo Frigerio (University of Warwick, UK) for sharing the αTIP-YFP reporter construct for all vacuoles and Gary Grafter (Faversham Institute of Biotechnology) for moral boosting and wedging spiritual support each Friday. F.B. was supported by a PhD international scholarship from the University of Leeds. This work was supported in part by the European Union (Project LSH-2002-1.2.5-2 "Recombinant Pharmaceuticals from Plants for Human Health Pharma-Planta") and by The Leverhulme Trust (F/10 105/E).

AUTHOR CONTRIBUTIONS

All authors performed research and analyzed data. F.B. and J.D. were also responsible for both experimental design and writing the article.

Received March 22, 2011; revised June 17, 2011; accepted July 14, 2011; published August 19, 2011.

REFERENCES

Abramoff, M.D., Magelhaes, P.J., and Ram, S.J. (2004). Image Processing with ImageJ. Biophotonics Int. **11:** 33–42.

Ahmed, S.U., Rojo, E., Kovaleva, V., Venkataraman, S., Dombrowski, J.E., Matsuoka, K., and Raikhel, N.V. (2000). The plant vacuolar sorting receptor AtELP is involved in transport of NH(2)-terminal propeptide-containing vacuolar proteins in *Arabidopsis thaliana*. J. Cell Biol. **149:** 1335–1344.

An, Q., Hückelhoven, R., Kogel, K.H., and van Bel, A.J. (2006). Multivesicular bodies participate in a cell wall-associated defence response in barley leaves attacked by the pathogenic powdery mildew fungus. Cell. Microbiol. **8:** 1009–1019.

An, Q., van Bel, A.J., and Hückelhoven, R. (2007). Do plant cells secrete exosomes derived from multivesicular bodies? Plant Signal. Behav. **2:** 4–7.

Bassham, D.C., Sanderfoot, A.A., Kovaleva, V., Zheng, H., and Raikhel, N.V. (2000). AtVPS45 complex formation at the *trans*-Golgi network. Mol. Biol. Cell **11:** 2251–2265.

Batistic, O., and Kudla, J. (2009). Plant calcineurin B-like proteins and their interacting protein kinases. Biochim. Biophys. Acta **1793:** 985–992.

Batistic, O., Waadt, R., Steinhorst, L., Held, K., and Kudla, J. (2010). CBL-mediated targeting of CIPKs facilitates the decoding of calcium signals emanating from distinct cellular stores. Plant J. **61:** 211–222.

Batoko, H., Zheng, H.-Q., Hawes, C., and Moore, I. (2000). A rab1 GTPase is required for transport between the endoplasmic reticulum and Golgi apparatus and for normal Golgi movement in plants. Plant Cell **12:** 2201–2218.

Bolte, S., Brown, S., and Satiat-Jeunemaitre, B. (2004). The N-myristoylated Rab-GTPase m-Rabmc is involved in post-Golgi trafficking events to the lytic vacuole in plant cells. J. Cell Sci. **117:** 943–954.

Cao, X., Rogers, S.W., Butler, J., Beevers, L., and Rogers, J.C. (2000). Structural requirements for ligand binding by a probable plant vacuolar sorting receptor. Plant Cell **12:** 493–506.

Chow, C.M., Neto, H., Foucart, C., and Moore, I. (2008). Rab-A2 and Rab-A3 GTPases define a trans-golgi endosomal membrane domain in *Arabidopsis* that contributes substantially to the cell plate. Plant Cell **20:** 101–123.

Chrispeels, M.J. (1983). The Golgi apparatus mediates the transport of phytohemagglutinin to the protein bodies in bean cotyledons. Planta **158:** 140–151.

Cowles, C.R., Odorizzi, G., Payne, G.S., and Emr, S.D. (1997). The AP-3 adaptor complex is essential for cargo-selective transport to the yeast vacuole. Cell **91:** 109–118.

Craddock, C.P., Hunter, P.R., Szakacs, E., Hinz, G., Robinson, D.G., and Frigerio, L. (2008). Lack of a vacuolar sorting receptor leads to non-specific missorting of soluble vacuolar proteins in Arabidopsis seeds. Traffic **9:** 408–416.

daSilva, L.L., Snapp, E.L., Denecke, J., Lippincott-Schwartz, J., Hawes, C., and Brandizzi, F. (2004). Endoplasmic reticulum export sites and Golgi bodies behave as single mobile secretory units in plant cells. Plant Cell **16:** 1753–1771.

daSilva, L.L., Taylor, J.P., Hadlington, J.L., Hanton, S.L., Snowden, C.J., Fox, S.J., Foresti, O., Brandizzi, F., and Denecke, J. (2005). Receptor salvage from the prevacuolar compartment is essential for efficient vacuolar protein targeting. Plant Cell **17:** 132–148.

De Matteis, M.A., and Luini, A. (2008). Exiting the Golgi complex. Nat. Rev. Mol. Cell Biol. **9:** 273–284.

Denecke, J., Botterman, J., and Deblaere, R. (1990). Protein secretion in plant cells can occur via a default pathway. Plant Cell **2:** 51–59.

Denecke, J., De Rycke, R., and Botterman, J. (1992). Plant and mammalian sorting signals for protein retention in the endoplasmic reticulum contain a conserved epitope. EMBO J. **11:** 2345–2355.

Dettmer, J., Hong-Hermesdorf, A., Stierhof, Y.D., and Schumacher, K. (2006). Vacuolar H+-ATPase activity is required for endocytic and secretory trafficking in *Arabidopsis*. Plant Cell **18:** 715–730.

Di Sansebastiano, G.P., Paris, N., Marc-Martin, S., and Neuhaus, J.-M. (2001). Regeneration of a lytic central vacuole and of neutral peripheral vacuoles can be visualized by green fluorescent proteins targeted to either type of vacuoles. Plant Physiol. **126:** 78–86.

Foresti, O., daSilva, L.L., and Denecke, J. (2006). Overexpression of the *Arabidopsis* syntaxin PEP12/SYP21 inhibits transport from the prevacuolar compartment to the lytic vacuole in vivo. Plant Cell **18:** 2275–2293.

Foresti, O., and Denecke, J. (2008). Intermediate organelles of the plant secretory pathway: Identity and function. Traffic **9:** 1599–1612.

Foresti, O., Gershlick, D.C., Bottanelli, F., Hummel, E., Hawes, C., and Denecke, J. (2010). A recycling-defective vacuolar sorting receptor reveals an intermediate compartment situated between prevacuoles and vacuoles in tobacco. Plant Cell **22:** 3992–4008.

French, A.P., Mills, S., Swarup, R., Bennett, M.J., and Pridmore, T.P. (2008). Colocalization of fluorescent markers in confocal microscope images of plant cells. Nat. Protoc. **3:** 619–628.

Frigerio, L., Hinz, G., and Robinson, D.G. (2008). Multiple vacuoles in plant cells: Rule or exception? Traffic **9:** 1564–1570.

Geldner, N. (2004). The plant endosomal system—Its structure and role in signal transduction and plant development. Planta **219:** 547–560.

Geldner, N., Anders, N., Wolters, H., Keicher, J., Kornberger, W., Muller, P., Delbarre, A., Ueda, T., Nakano, A., and Jürgens, G. (2003). The Arabidopsis GNOM ARF-GEF mediates endosomal recycling, auxin transport, and auxin-dependent plant growth. Cell **112:** 219–230.

Gomez, L., and Chrispeels, M.J. (1993). Tonoplast and soluble vacuolar proteins are targeted by different mechanisms. Plant Cell **5:** 1113–1124.

Haas, A., Scheglmann, D., Lazar, T., Gallwitz, D., and Wickner, W. (1995). The GTPase Ypt7p of *Saccharomyces cerevisiae* is required on both partner vacuoles for the homotypic fusion step of vacuole inheritance. EMBO J. **14:** 5258–5270.

Hadlington, J.L., and Denecke, J. (2000). Sorting of soluble proteins in the secretory pathway of plants. Curr. Opin. Plant Biol. **3:** 461–468.

Harsay, E., and Schekman, R. (2002). A subset of yeast vacuolar protein sorting mutants is blocked in one branch of the exocytic pathway. J. Cell Biol. **156:** 271–285.

Hohl, I., Robinson, D.G., Chrispeels, M.J., and Hinz, G. (1996). Transport of storage proteins to the vacuole is mediated by vesicles without a clathrin coat. J. Cell Sci. **109:** 2539–2550.

Hunter, P.R., Craddock, C.P., Di Benedetto, S., Roberts, L.M., and Frigerio, L. (2007). Fluorescent reporter proteins for the tonoplast and the vacuolar lumen identify a single vacuolar compartment in Arabidopsis cells. Plant Physiol. **145:** 1371–1382.

Isayenkov, S., Isner, J.C., and Maathuis, F.J. (2011). Rice two-pore K+ channels are expressed in different types of vacuoles. Plant Cell **23:** 756–768.

Jones, S., Litt, R.J., Richardson, C.J., and Segev, N. (1995). Requirement of nucleotide exchange factor for Ypt1 GTPase mediated protein transport. J. Cell Biol. **130:** 1051–1061.

Kirsch, T., Paris, N., Butler, J.M., Beevers, L., and Rogers, J.C. (1994). Purification and initial characterization of a potential plant vacuolar targeting receptor. Proc. Natl. Acad. Sci. USA **91:** 3403–3407.

Kirsch, T., Saalbach, G., Raikhel, N.V., and Beevers, L. (1996). Interaction of a potential vacuolar targeting receptor with amino- and carboxyl-terminal targeting determinants. Plant Physiol. **111:** 469–474.

Kotzer, A.M., Brandizzi, F., Neumann, U., Paris, N., Moore, I., and Hawes, C. (2004). AtRabF2b (Ara7) acts on the vacuolar trafficking pathway in tobacco leaf epidermal cells. J. Cell Sci. **117:** 6377–6389.

Lam, S.K., Cai, Y., Tse, Y.C., Wang, J., Law, A.H., Pimpl, P., Chan, H.Y., Xia, J., and Jiang, L. (2009). BFA-induced compartments from the Golgi apparatus and trans-Golgi network/early endosome are distinct in plant cells. Plant J. **60:** 865–881.

Lee, G.J., Sohn, E.J., Lee, M.H., and Hwang, I. (2004). The Arabidopsis rab5 homologs rha1 and ara7 localize to the prevacuolar compartment. Plant Cell Physiol. **45:** 1211–1220.

Lippincott-Schwartz, J., Yuan, L.C., Bonifacino, J.S., and Klausner, R.D. (1989). Rapid redistribution of Golgi proteins into the ER in cells treated with brefeldin A: Evidence for membrane cycling from Golgi to ER. Cell **56:** 801–813.

Luan, S., Kudla, J., Rodriguez-Concepcion, M., Yalovsky, S., and Gruissem, W. (2002). Calmodulins and calcineurin B-like proteins: Calcium sensors for specific signal response coupling in plants. Plant Cell **14** (suppl.): S389–S400.

Maliga, P., Sz-Breznovits, A., and Márton, L. (1973). Streptomycin-resistant plants from callus culture of haploid tobacco. Nat. New Biol. **244:** 29–30.

Matsuoka, K., Bassham, D.C., Raikhel, N.V., and Nakamura, K. (1995). Different sensitivity to wortmannin of two vacuolar sorting signals indicates the presence of distinct sorting machineries in tobacco cells. J. Cell Biol. **130:** 1307–1318.

Matsuoka, K., and Nakamura, K. (1999). Large alkyl side-chains of isoleucine and leucine in the NPIRL region constitute the core of the vacuolar sorting determinant of sporamin precursor. Plant Mol. Biol. **41:** 825–835.

Mazel, A., Leshem, Y., Tiwari, B.S., and Levine, A. (2004). Induction of salt and osmotic stress tolerance by overexpression of an intracellular vesicle trafficking protein AtRab7 (AtRabG3e). Plant Physiol. **134:** 118–128.

Miao, Y., Li, K.Y., Li, H.Y., Yao, X., and Jiang, L. (2008). Vacuolar transport of aleurain-GFP and 2S albumin-GFP fusions is mediated by the same prevacuolar compartments in tobacco BY-2 and Arabidopsis suspension cultured cells. Plant J. **56:** 824–839.

Murashige, R., and Skoog, F. (1962). A revised medium for rapid growth and bioassays with tobacco tissue cultures. Physiol. Plant. **15:** 473–497.

Nahm, M.Y., Kim, S.W., Yun, D., Lee, S.Y., Cho, M.J., and Bahk, J.D. (2003). Molecular and biochemical analyses of OsRab7, a rice Rab7 homolog. Plant Cell Physiol. **44:** 1341–1349.

Neuhaus, J.M., Sticher, L., Meins, F., Jr., and Boller, T. (1991). A short C-terminal sequence is necessary and sufficient for the targeting of chitinases to the plant vacuole. Proc. Natl. Acad. Sci. USA **88:** 10362–10366.

Niemes, S., Labs, M., Scheuring, D., Krueger, F., Langhans, M., Jesenofsky, B., Robinson, D.G., and Pimpl, P. (2010). Sorting of plant vacuolar proteins is initiated in the ER. Plant J. **62:** 601–614.

Osterrieder, A., Carvalho, C.M., Latijnhouwers, M., Johansen, J.N., Stubbs, C., Botchway, S., and Hawes, C. (2009). Fluorescence lifetime imaging of interactions between Golgi tethering factors and small GTPases in plants. Traffic **10:** 1034–1046.

Paris, N., Stanley, C.M., Jones, R.L., and Rogers, J.C. (1996). Plant cells contain two functionally distinct vacuolar compartments. Cell **85:** 563–572.

Pelchen-Matthews, A., Raposo, G., and Marsh, M. (2004). Endosomes, exosomes and Trojan viruses. Trends Microbiol. **12:** 310–316.

Peyroche, A., Antonny, B., Robineau, S., Acker, J., Cherfils, J., and Jackson, C.L. (1999). Brefeldin A acts to stabilize an abortive ARF-GDP-Sec7 domain protein complex: Involvement of specific residues of the Sec7 domain. Mol. Cell **3:** 275–285.

Phillipson, B.A., Pimpl, P., daSilva, L.L., Crofts, A.J., Taylor, J.P., Movafeghi, A., Robinson, D.G., and Denecke, J. (2001). Secretory bulk flow of soluble proteins is efficient and COPII dependent. Plant Cell **13:** 2005–2020.

Pimpl, P., Hanton, S.L., Taylor, J.P., Pinto-daSilva, L.L., and Denecke, J. (2003). The GTPase ARF1p controls the sequence-specific vacuolar sorting route to the lytic vacuole. Plant Cell **15:** 1242–1256.

Pimpl, P., Taylor, J.P., Snowden, C.J., Hillmer, S., Robinson, D.G., and Denecke, J. (2006). Golgi-mediated vacuolar sorting of the endoplasmic reticulum chaperone bip may play an active role in quality control within the secretory pathway. Plant Cell **18:** 198–211.

Preuss, M.L., Schmitz, A.J., Thole, J.M., Bonner, H.K., Otegui, M.S., and Nielsen, E. (2006). A role for the RabA4b effector protein PI-4Kbeta1 in polarized expansion of root hair cells in *Arabidopsis thaliana*. J. Cell Biol. **172:** 991–998.

Preuss, M.L., Serna, J., Falbel, T.G., Bednarek, S.Y., and Nielsen, E. (2004). The *Arabidopsis* Rab GTPase RabA4b localizes to the tips of growing root hair cells. Plant Cell **16:** 1589–1603.

Richardson, C.J., Jones, S., Litt, R.J., and Segev, N. (1998). GTP hydrolysis is not important for Ypt1 GTPase function in vesicular transport. Mol. Cell. Biol. **18:** 827–838.

Rutherford, S., and Moore, I. (2002). The Arabidopsis Rab GTPase family: Another enigma variation. Curr. Opin. Plant Biol. **5:** 518–528.

Saalbach, G., Rosso, M., and Schumann, U. (1996). The vacuolar targeting signal of the 2S albumin from Brazil nut resides at the C terminus and involves the C-terminal propeptide as an essential element. Plant Physiol. **112:** 975–985.

Saint-Jean, B., Seveno-Carpentier, E., Alcon, C., Neuhaus, J.M., and Paris, N. (2010). The cytosolic tail dipeptide Ile-Met of the pea receptor BP80 is required for recycling from the prevacuole and for endocytosis. Plant Cell **22:** 2825–2837.

Saito, C., Ueda, T., Abe, H., Wada, Y., Kuroiwa, T., Hisada, A., Furuya, M., and Nakano, A. (2002). A complex and mobile structure forms a distinct subregion within the continuous vacuolar membrane in young cotyledons of Arabidopsis. Plant J. **29:** 245–255.

Sanderfoot, A.A., Kovaleva, V., Bassham, D.C., and Raikhel, N.V. (2001). Interactions between syntaxins identify at least five SNARE complexes within the Golgi/prevacuolar system of the Arabidopsis cell. Mol. Biol. Cell **12:** 3733–3743.

Sanmartín, M., Ordóñez, A., Sohn, E.J., Robert, S., Sánchez-Serrano, J.J., Surpin, M.A., Raikhel, N.V., and Rojo, E. (2007). Divergent functions of VTI12 and VTI11 in trafficking to storage and lytic vacuoles in Arabidopsis. Proc. Natl. Acad. Sci. USA **104:** 3645–3650.

Shimada, T., Fuji, K., Tamura, K., Kondo, M., Nishimura, M., and Hara-Nishimura, I. (2003). Vacuolar sorting receptor for seed storage proteins in *Arabidopsis thaliana.* Proc. Natl. Acad. Sci. USA **100:** 16095–16100.

Sohn, E.J., Kim, E.S., Zhao, M., Kim, S.J., Kim, H., Kim, Y.W., Lee, Y.J., Hillmer, S., Sohn, U., Jiang, L., and Hwang, I. (2003). Rha1, an *Arabidopsis* Rab5 homolog, plays a critical role in the vacuolar trafficking of soluble cargo proteins. Plant Cell **15:** 1057–1070.

Sparkes, I.A., Runions, J., Kearns, A., and Hawes, C. (2006). Rapid, transient expression of fluorescent fusion proteins in tobacco plants and generation of stably transformed plants. Nat. Protoc. **1:** 2019–2025.

Speth, E.B., Imboden, L., Hauck, P., and He, S.Y. (2009). Subcellular localization and functional analysis of the Arabidopsis GTPase RabE. Plant Physiol. **149:** 1824–1837.

Staehelin, L.A., and Kang, B.H. (2008). Nanoscale architecture of endoplasmic reticulum export sites and of Golgi membranes as determined by electron tomography. Plant Physiol. **147:** 1454–1468.

Szumlanski, A.L., and Nielsen, E. (2009). The Rab GTPase RabA4d regulates pollen tube tip growth in *Arabidopsis thaliana*. Plant Cell **21:** 526–544.

Théry, C., Zitvogel, L., and Amigorena, S. (2002). Exosomes: Composition, biogenesis and function. Nat. Rev. Immunol. **2:** 569–579.

Toyooka, K., Goto, Y., Asatsuma, S., Koizumi, M., Mitsui, T., and Matsuoka, K. (2009). A mobile secretory vesicle cluster involved in mass transport from the Golgi to the plant cell exterior. Plant Cell **21:** 1212–1229.

Ueda, T., Anai, T., Tsukaya, H., Hirata, A., and Uchimiya, H. (1996). Characterization and subcellular localization of a small GTP-binding protein (Ara-4) from Arabidopsis: Conditional expression under control of the promoter of the gene for heat-shock protein HSP81-1. Mol. Gen. Genet. **250:** 533–539.

Ueda, T., Yamaguchi, M., Uchimiya, H., and Nakano, A. (2001). Ara6, a plant-unique novel type Rab GTPase, functions in the endocytic pathway of *Arabidopsis thaliana*. EMBO J. **20:** 4730–4741.

Uemura, T., Morita, M.T., Ebine, K., Okatani, Y., Yano, D., Saito, C., Ueda, T., and Nakano, A. (2010). Vacuolar/pre-vacuolar compartment Qa-SNAREs VAM3/SYP22 and PEP12/SYP21 have interchangeable functions in Arabidopsis. Plant J. **64:** 864–873.

Uemura, T., Yoshimura, S.H., Takeyasu, K., and Sato, M.H. (2002). Vacuolar membrane dynamics revealed by GFP-AtVam3 fusion protein. Genes Cells **7:** 743–753.

Ullrich, O., Reinsch, S., Urbé, S., Zerial, M., and Parton, R.G. (1996). Rab11 regulates recycling through the pericentriolar recycling endosome. J. Cell Biol. **135:** 913–924.

Velten, J., Velten, L., Hain, R., and Schell, J. (1984). Isolation of a dual plant promoter fragment from the Ti plasmid of *Agrobacterium tumefaciens*. EMBO J. **3:** 2723–2730.

Viotti, C., et al. (2010). Endocytic and secretory traffic in *Arabidopsis* merge in the trans-Golgi network/early endosome, an independent and highly dynamic organelle. Plant Cell **22:** 1344–1357.

von Heijne, G., and Gavel, Y. (1988). Topogenic signals in integral membrane proteins. Eur. J. Biochem. **174:** 671–678.

Wang, J., Cai, Y., Miao, Y., Lam, S.K., and Jiang, L. (2009). Wortmannin induces homotypic fusion of plant prevacuolar compartments. J. Exp. Bot. **60:** 3075–3083.

Zheng, H., Camacho, L., Wee, E., Batoko, H., Legen, J., Leaver, C.J., Malhó, R., Hussey, P.J., and Moore, I. (2005). A Rab-E GTPase mutant acts downstream of the Rab-D subclass in biosynthetic membrane traffic to the plasma membrane in tobacco leaf epidermis. Plant Cell **17:** 2020–2036.

Zouhar, J., Muñoz, A., and Rojo, E. (2010). Functional specialization within the vacuolar sorting receptor family: VSR1, VSR3 and VSR4 sort vacuolar storage cargo in seeds and vegetative tissues. Plant J. **64:** 577–588.

Zouhar, J., Rojo, E., and Bassham, D.C. (2009). AtVPS45 is a positive regulator of the SYP41/SYP61/VTI12 SNARE complex involved in trafficking of vacuolar cargo. Plant Physiol. **149:** 1668–1678.